THE OPERATIONAL NUMERICAL WEATHER PREDICTION MODEL

by

A. DICKINSON and
C. TEMPERTON

MET O 11 TECHNICAL NOTE No 183

THE OPERATIONAL NUMERICAL WEATHER PREDICTION MODEL

by

A. Dickinson and C. Temperton

January 1984

Met O 11 (Forecasting Research)
Meteorological Office
London Rd
Bracknell
Berkshire

CONTENTS.

1. INTRODUCTION

In August 1982, after ten years of service, the Meteorological Office's 10-level hemispheric "octagon" numerical weather prediction model (Burridge and Gadd, 1977) was withdrawn from daily operational use, to be replaced by a new global 15-level model run on the recently aquired Cyber 205 computer. In the following month the old regional "rectangle" model, covering a smaller area on a finer mesh and used principally for 36-hour predictions of the weather in the neighbourhood of the United Kingdom, was replaced by a new fine mesh model.

The design of the new models followed a period of research aimed at identifying the most important ingredients for a successful short-to-medium range prediction model. The results of this research (Cullen et al., 1981) suggested that none of the possible discretization techniques, that is finite-difference, spectral or finite-element, showed any clear advantage over the others, and the design strategy was thus to implement a simple economical model with as high a resolution as computer resources would reasonably allow.

A split-explicit finite-difference scheme (Gadd, 1978a) is used to integrate the governing prognostic equations for momentum, temperature and humidity, together with the continuity and hydrostatic equations. Because of the global coverage required of the coarse mesh model, these equations are defined on a latitude-longitude grid. The non-dimensional variable $\sigma = p/p_*$ is used as the vertical coordinate. The physical processes modelled are large-scale precipitation, deep-convection, radiation and the vertical transfer of heat, moisture and momentum through the atmospheric boundary layer. The techniques used here were developed over a period of several years for use in the Meteorological Office's 11-layer general circulation model (Saker, 1975) and have been adapted for short-to-medium range forecasting.

The purpose of this paper is primarily to document the formulation

and design of the new operational models, including the modifications made in the light of experience up to January 1984. Its contents are also applicable to the research versions of these models such as the 11-level low resolution global model used for long range forecasting studies and the experimental higher resolution versions of the fine mesh model.

The forecast models themselves form only a part of the operational suite; just as important are the data assimilation scheme used to define initial conditions for the model forecasts, and the translation of the results into various output media for supply to users. A companion paper (Lyne et al., 1983) describes the current design of the operational data assimilation scheme.

2. THE CO-ORDINATE SYSTEM AND CONTINUOUS EQUATIONS.

2.1 The horizontal co-ordinate system.

In the old "octagon" operational model, with its southern boundary near 10° N, the equations were written in terms of a cartesian (x,y) co-ordinate system on a polar stereographic projection. Since the new model is required to produce global forecasts, such a co-ordinate system could no longer be used as the south pole would be at infinity. The new model is therefore based on a spherical polar co-ordinate system with latitude ϕ and longitude λ as the independent variables.

For a global model, no horizontal boundary conditions are required. The lateral boundary conditions for the hemispheric, 30° S and fine mesh models are described in Section 10.

2.2 The vertical co-ordinate system.

The old operational models used a pressure co-ordinate system in the vertical. Although this system worked well enough, it had the disadvantage that the lower pressure levels disappeared below high topography, and in the case of the 1000 mb surface this even occured at sea-level in regions of low surface pressure.

In order to avoid such problems the new models use a sigma co-ordinate in the vertical, defined by $\sigma = p/p_*$ where p is pressure and p_* is surface pressure (Phillips, 1957). The surface of the earth is therefore always at $\sigma = 1$, resulting in simple boundary conditions, while the top of the atmosphere, where $p = 0$, is at $\sigma = 0$.

The vertical boundary conditions are simply

$$\dot{\sigma} = 0 \quad \text{at} \quad \sigma = 0, 1 \qquad (2.1)$$

where $\dot{\sigma} = \frac{d\sigma}{dt}$, is the vertical velocity in sigma co-ordinates.

2.3 The continuous equations.

In the (λ, ϕ, σ) co-ordinate system, the momentum equations may be written as follows:

$$\frac{\partial u}{\partial t} + \frac{u}{a\cos\phi}\frac{\partial u}{\partial \lambda} + \frac{v}{a}\frac{\partial u}{\partial \phi} + \dot{\sigma}\frac{\partial u}{\partial \sigma} - \left(f + \frac{u\tan\phi}{a}\right)v + \frac{1}{a\cos\phi}\left(\frac{\partial \Phi}{\partial \lambda} + c_p\sigma^{\kappa}\theta\frac{\partial \tilde{\Pi}}{\partial \lambda}\right) = \mathbb{F}_u \qquad (2.2)$$

$$\frac{\partial v}{\partial t} + \frac{u}{a\cos\phi}\frac{\partial v}{\partial \lambda} + \frac{v}{a}\frac{\partial v}{\partial \phi} + \dot{\sigma}\frac{\partial v}{\partial \sigma} + \left(f + \frac{u\tan\phi}{a}\right)u + \frac{1}{a}\left(\frac{\partial \Phi}{\partial \phi} + c_p\sigma^{\kappa}\theta\frac{\partial \tilde{\Pi}}{\partial \phi}\right) = \mathbb{F}_v \qquad (2.3)$$

where a is the radius of the earth, f is the coriolis parameter, Φ is the geopotential, c_p is the specific heat of air and θ is potential temperature. $\tilde{\Pi}$, the Exner surface pressure, is given by

$$\tilde{\Pi} = \left(\frac{p_*}{1000}\right)^{\kappa}$$

where $\kappa = R/c_p$ and R is the gas constant. The terms $\mathbb{F}_u$ and $\mathbb{F}_v$ represent sources and sinks of momentum due to the subgridscale effects described in Sections 5-8, together with dissipation terms.

The thermodynamic equation is

$$\frac{\partial \theta}{\partial t} + \frac{u}{a\cos\phi}\frac{\partial \theta}{\partial \lambda} + \frac{v}{a}\frac{\partial \theta}{\partial \phi} + \dot{\sigma}\frac{\partial \theta}{\partial \sigma} = \mathbb{F}_\theta \qquad (2.4)$$

and the moisture equation is

$$\frac{\partial r}{\partial t} + \frac{u}{a\cos\phi}\frac{\partial r}{\partial \lambda} + \frac{v}{a}\frac{\partial r}{\partial \phi} + \dot{\sigma}\frac{\partial r}{\partial \sigma} = \mathcal{F}_r \qquad (2.5)$$

where θ is potential temperature, r is specific humidity, and $\mathcal{F}_\theta$ and $\mathcal{F}_r$ represent sources and sinks of heat and moisture respectively.

The continuity equation in sigma co-ordinates is

$$\frac{\partial p_*}{\partial t} + \frac{1}{a\cos\phi}\left(\frac{\partial}{\partial \lambda}(p_* u) + \frac{\partial}{\partial \phi}(p_* v\cos\phi)\right) + \frac{\partial}{\partial \sigma}(p_*\dot{\sigma}) = 0 \qquad (2.6)$$

which, when integrated vertically using the boundary conditions (2.1), gives a predictive equation for the surface pressure,

$$\frac{\partial p_*}{\partial t} + \frac{1}{a\cos\phi}\int_0^1 \left[\frac{\partial}{\partial \lambda}(p_* u) + \frac{\partial}{\partial \phi}(p_* v\cos\phi)\right] d\sigma = 0 \qquad (2.7)$$

The vertical velocity $\dot{\sigma}$ is also given by integrating (2.6):

$$p_*\dot{\sigma} = -\frac{1}{a\cos\phi}\int_0^\sigma \left[\frac{\partial}{\partial \lambda}(p_* u) + \frac{\partial}{\partial \phi}(p_* v\cos\phi)\right] d\sigma - \sigma\frac{\partial p_*}{\partial t} \qquad (2.8)$$

The geopotential Φ is determined from the hydrostatic equation:

$$\frac{\partial \Phi}{\partial \sigma} + \frac{R T_v}{\sigma} = 0 \qquad (2.9)$$

where T_v is virtual temperature, given by $T_v = T(1 + 0.61r)$, and the temperature is related to potential temperature θ by

$$T = \left(\frac{p}{1000}\right)^\kappa \theta \qquad (2.10)$$

3. THE MODEL GRIDS.

3.1 The horizontal grid

In the horizontal we use a regular grid defined by intersections of lines of latitude and longitude. For the coarse-mesh model, the grid increments are given by $\Delta\lambda = 1.875^\circ$ and $\Delta\phi = 1.5^\circ$. This means that there are 192 points around each latitude circle and 121 rows from north pole to south pole.

The area covered by the operational fine-mesh model is shown in Figure 3.1. It is enclosed by the longitude lines 80.625° W and 39.375° E, and by the latitude lines 79.5° N and 30° N. The grid increments for the fine mesh model are $\Delta\lambda = 0.9375^\circ$ and $\Delta\phi = 0.75^\circ$, that is twice the resolution of the coarse mesh model. The dimensions of the fine-mesh area are thus 129 points E-W and 67 N-S.

The variables are horizontally staggered using the arrangement of the so called "B" grid (Arakawa, 1966). Thus the wind components (u,v) are held at points $((i+\frac{1}{2})\Delta\lambda,\ (j+\frac{1}{2})\Delta\phi)$ whilst the remaining variables p*, θ, r, together with the diagnostic quantities $\dot{\sigma}$ and Φ, are held at the points $(i\Delta\lambda, j\Delta\phi)$. See Figure 3.2.

3.2 The vertical grid

The 15 σ-levels used operationally are unequally spaced, in order to give higher resolution in the boundary layer and in the vicinity of the tropopause and jet streams. The prognostic variables u, v, θ, r and the geopotential Φ are held at the levels σ_K while the vertical velocity is held at the intermediate levels $\sigma_{K+\frac{1}{2}}$. The σ-values of these levels are given in Table 3.1.

Number	Full-level	Half-level
		0.013
15	0.025	
		0.042
14	0.065	
		0.098
13	0.125	
		0.156
12	0.190	
		0.228
11	0.250	
		0.273
10	0.310	
		0.350
9	0.390	
		0.433
8	0.490	
		0.552
7	0.590	
		0.630
6	0.690	
		0.754
5	0.790	
		0.827
4	0.870	
		0.914
3	0.935	
		0.956
2	0.975	
		0.994
1	0.997	

Table 3.1 The σ-levels used by the operational forecast models.

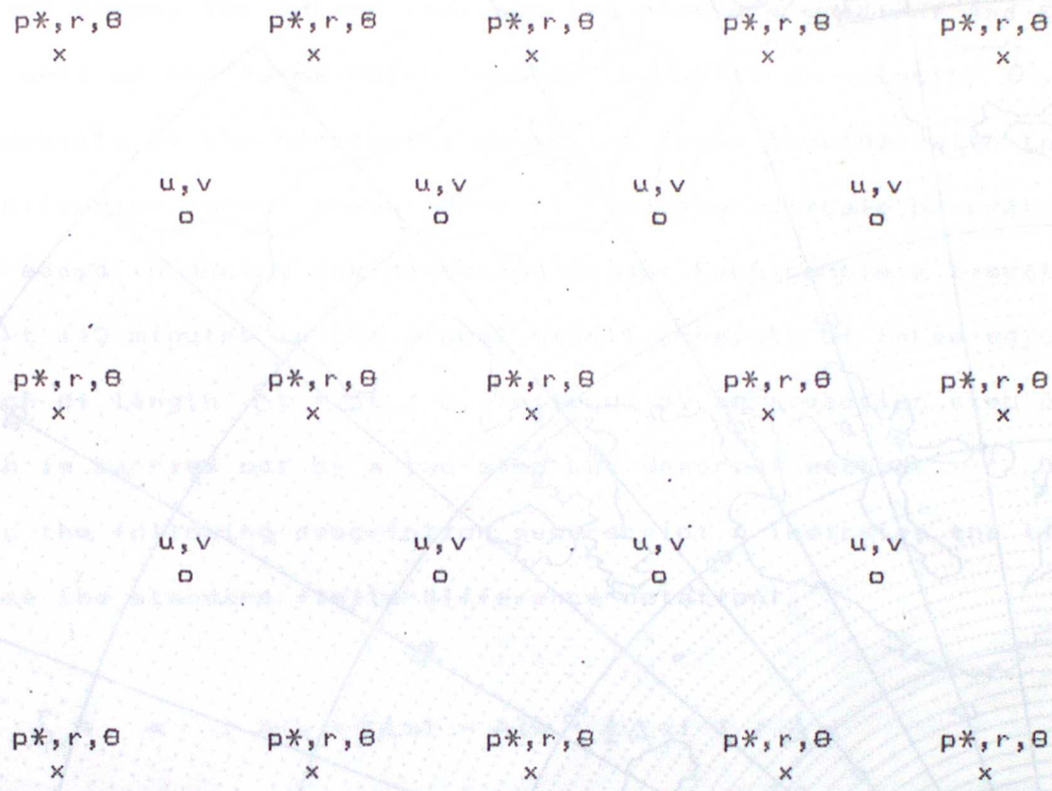

Figure 3.2 The horizontal grid spacing used in the operatioanl models.

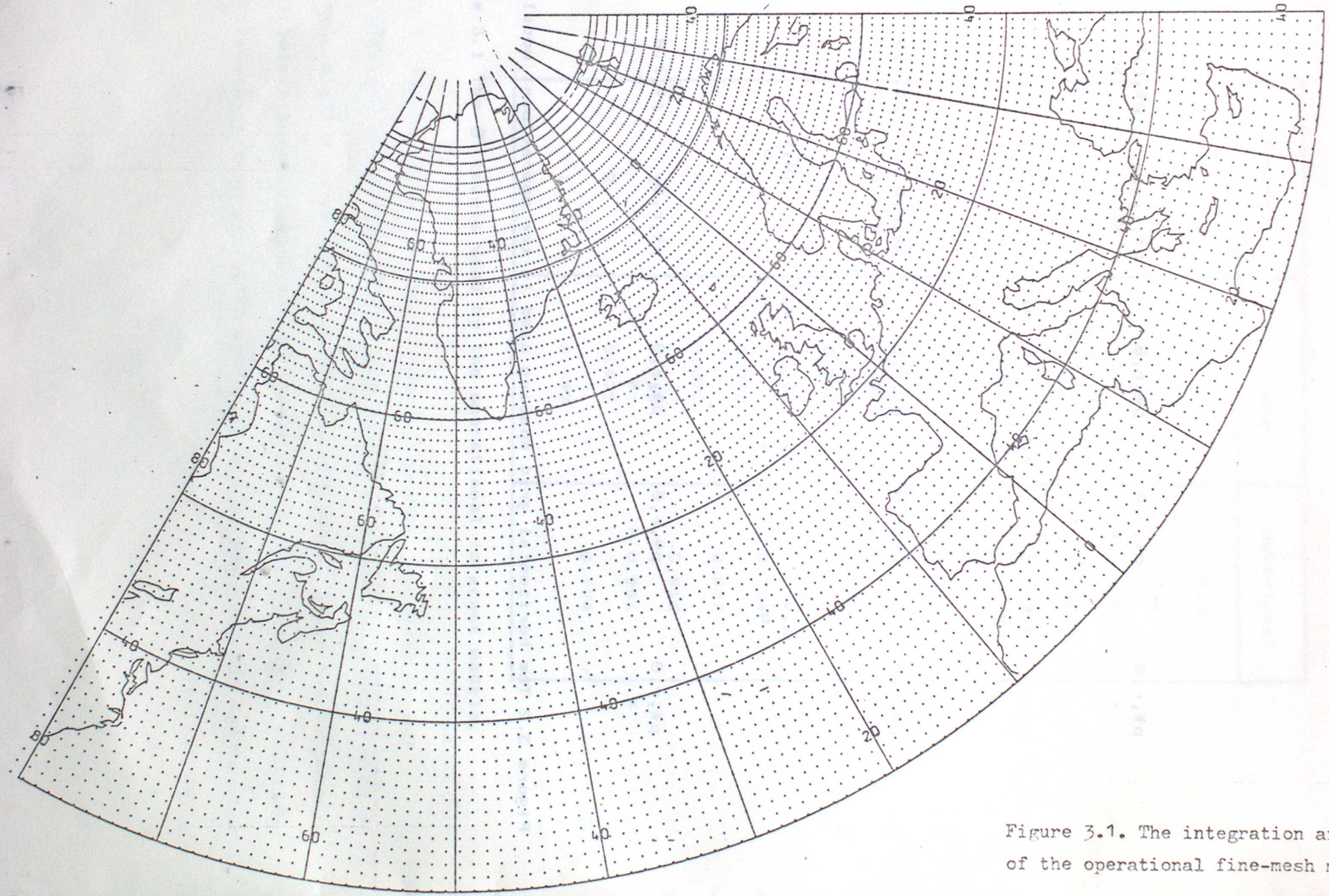

Figure 3.1. The integration area of the operational fine-mesh model.

4. THE INTEGRATION SCHEME.

The model uses an economical split-explicit integration scheme similar to that introduced by Gadd (1978a) for the 10-level model. The equations are split into two parts, called the "adjustment" and "advection" steps. The former includes the pressure gradient and Coriolis terms as well as the terms which involve the vertical velocity $\dot{\sigma}$, and the latter consists of the horizontal advection terms together with the lateral diffusion terms. The effects of the subgrid-scale parametrizations are also added in during the advection stage. Each complete timestep of length Δt (15 minutes in the global model) consists of three adjustment steps each of length $\delta t = \Delta t / 3$, followed by an advection step of length Δt which is carried out by a two-step Lax-Wendroff method.

In the following description superscript n indicates the time level and we use the standard finite-difference notation:

$$\delta_x A = [\, A(x + \tfrac{1}{2}\Delta x) - A(x - \tfrac{1}{2}\Delta x) \,] / \Delta x$$

$$\overline{A}^{x} = [\, A(x + \tfrac{1}{2}\Delta x) + A(x - \tfrac{1}{2}\Delta x) \,] / 2$$

4.1 The adjustment step.

The adjustment step uses a "forward-backward" scheme in which a forward difference in time is used for the p*, θ, and r equations, and the new values of these variables are then used in the u and v equations The "forward" part of the integration scheme is:

$$p_*^{n+1} - p_*^{n} = \frac{-\delta t}{a \cos\phi} \left[\delta_\lambda \left(\overline{p_*}^{\lambda\phi} \sum_{\ell=1}^{\text{Top}} u_\ell (\Delta\sigma)_\ell \right)^{\phi} + \delta_\phi \left(\cos\phi \, \overline{p_*}^{\lambda\phi} \sum_{\ell=1}^{\text{Top}} v_\ell (\Delta\sigma)_\ell \right)^{\lambda} \right]^{n} \qquad (4.1)$$

$$\theta^{n+1} - \theta^{n} = -\delta t \left[\dot{\sigma} \frac{\partial \theta}{\partial \sigma} \right]^{n} \qquad (4.2)$$

$$r^{n+1} - r^{n} = -\delta t \left[\dot{\sigma} \frac{\partial r}{\partial \sigma} \right]^{n} \qquad (4.3)$$

The vertical advection terms in (4.2) and (4.3) must be carefully handled to ensure the correct balancing of energy conversions. The finite-difference form which conserves heat is given by

$$\dot{\sigma} \frac{\partial \theta}{\partial \sigma} = \frac{1}{(\Delta\sigma)_K} \left[(\sigma_K - \sigma_{K-\frac{1}{2}}) [\dot{\sigma} \delta_\sigma \theta]_{K-\frac{1}{2}} + (\sigma_{K+\frac{1}{2}} - \sigma_K) [\dot{\sigma} \delta_\sigma \theta]_{K+\frac{1}{2}} \right] \qquad (4.4)$$

in (4.2) with a similar expression in (4.3).

The vertical velocity $\dot{\sigma}$ is given by

$$(P_* \dot{\sigma})_{K+\frac{1}{2}} = \frac{-1}{a \cos\phi} \left(\sum_{n=1}^{K} - \sigma_{K+\frac{1}{2}} \sum_{\ell=1}^{TOP} \right) \left[\delta_\lambda \left(\overline{P_*}^{\lambda\phi} u \right)^{\phi} + \delta_\phi \left(\overline{\cos\phi \, \overline{P_*}^{\lambda\phi} v} \right)^{\lambda} \right]_\ell (\Delta\sigma)_\ell \qquad (4.5)$$

The "backward" part of the integration scheme is given by

$$u^{n+1} - u^{n} = \delta t \left[\tfrac{1}{2} F \left(v^{n} + v^{n+1} \right) - \overline{\dot{\sigma}^{n}}^{\lambda\phi} \overline{\delta_\sigma u^{n}}^{\sigma} \right.$$

$$\left. - \frac{1}{a \cos\phi} \left(\delta_\lambda \Phi^{n+1} + c_p \overline{\sigma^{K} \left(\bar{\theta}^{\lambda} \delta_\lambda \Pi \right)^{n+1}}^{\phi} \right) \right] \qquad (4.6)$$

$$v^{n+1} - v^{n} = \delta t \left[\tfrac{1}{2} F \left(u^{n} + u^{n+1} \right) - \overline{\dot{\sigma}^{n}}^{\lambda\phi} \overline{\delta_\sigma v^{n}}^{\sigma} \right.$$

$$\left. - \frac{1}{a} \left(\delta_\phi \Phi^{n+1} + c_p \overline{\sigma^{K} \left(\bar{\theta}^{\phi} \delta_\phi \Pi \right)^{n+1}}^{\lambda} \right) \right] \qquad (4.7)$$

where $F = (f + u \tan\phi / a)$.

Note that the vertical advection terms in equations (4.6) and (4.7)

are handled in a "forward" manner, which in theory would eventually lead to instability. In practice, however, the amplification is compensated by damping elsewhere in the scheme.

The coriolis terms in equations (4.6) and (4.7) are handled by a centred implicit step in order to eliminate a source of instability noted by Gadd (1980); this is essential for integrations of more than a few days.

The geopotential $\bar{\Phi}$ required in equations (4.6) and (4.7) is computed by the following discrete form of the hydrostatic equation:

$$\bar{\Phi}_K = \bar{\Phi}_* + \sum_{\ell=1}^{K-1} R\,(T_v)_\ell \ln\left(\frac{\sigma_{\ell-\frac{1}{2}}}{\sigma_{\ell+\frac{1}{2}}}\right) + R\,(T_v)_K \ln\left(\frac{\sigma_K}{\sigma_{K+\frac{1}{2}}}\right) \qquad (4.8)$$

where $\bar{\Phi}_*$ is the orographic height.

4.2 Grid splitting.

The difference scheme described above can suffer from a grid separation, since the "B" grid supports two independent solutions. This instability can be forced by boundaries and experience has shown that its effects are more apparent in limited area versions of the model. To prevent this decoupling, a scheme devised by Mesinger (1973) and extended by Janjic (1979) is used, and is applied in slightly different forms in the fine-mesh and coarse-mesh versions of the model.

A term of the form

$$w\,\delta t^2 \sum_{K=1}^{ToP} (\nabla_+^2 - \nabla_\times^2)\, P_K\, (\Delta\sigma)_K$$

is added to the right-hand side of equation (4.1) in all versions of the model, where

$$\nabla_+^2 P_K = \frac{1}{a^2\cos^2\phi}\left[\delta_\lambda\left(\bar{P}_*^\lambda \delta_\lambda \bar{\Phi}\right) + \delta_\lambda\left(c_p \bar{\theta}^\lambda \sigma^\kappa \bar{P}_*^\lambda \delta_\lambda \Pi\right)\right]$$

$$+ \frac{1}{a^2\cos\phi}\left[\delta_\phi\left(\cos\phi\,\bar{P}_*^{\phi}\delta_\phi\Phi\right) + \delta_\phi\left(\cos\phi\, c_p\bar{\theta}^{\phi}\sigma^{k}\bar{P}_*^{\phi}\delta_\phi\tilde{\Pi}\right)\right]$$

(4.9)

$$\nabla_x^2 P_k = \frac{1}{a^2\cos^2\phi}\left[\overline{\delta_\lambda\left(\bar{P}_*^{\lambda\phi}\overline{\delta_\lambda\Phi}^{\phi}\right)}^{\phi} + \overline{\delta_\lambda\left(c_p\bar{P}_*^{\lambda\phi}\sigma^{k}\,\overline{\bar{\theta}^{\lambda}\delta_\lambda\tilde{\Pi}}^{\phi}\right)}^{\phi}\right]$$

$$+ \frac{1}{a^2\cos\phi}\left[\overline{\delta_\phi\left(\cos\phi\,\bar{P}_*^{\lambda\phi}\overline{\delta_\phi\Phi}^{\lambda}\right)}^{\lambda} + \overline{\delta_\phi\left(\cos\phi\,\bar{P}_*^{\lambda\phi}c_p\sigma^{k}\,\overline{\bar{\theta}^{\phi}\delta_\phi\tilde{\Pi}}^{\lambda}\right)}^{\lambda}\right]$$

This couples the external gravity mode by ensuring that perturbations in the height field are immediately felt at all the surrounding gridpoints.

In the fine mesh model the internal gravity modes are also coupled in a similar fashion, a term of the form

$$w\,\delta t^2 \sum_{l=1}^{l=k}\left(\nabla_+^2 - \nabla_x^2\right)P_l\,(\Delta\sigma)_l$$

being added to the righthand side of equation (4.5)

An upper limit for the value of the parameter w may be inferred from linear stability theory. (See Appendix A). The maximum allowed for stability is w = 0.25. At present a value of w = 0·125 is used in all versions of the model.

4.3 The advection step.

The two-step Lax-Wendroff integration scheme for the advection step uses the modification due to Gadd (1978b, 1980), which gives smaller phase and amplitude errors. The scheme is "time-staggered" with the variables (θ, r) and (u, v) changing places at the end of the first step. The finite-difference equations for the first step are:

$$\theta^{n+\frac{1}{2}} = \left[\bar{\theta}^{\lambda\phi} - \tfrac{1}{2}\Delta t\left(\frac{u}{a\cos\phi}\delta_\lambda\bar{\theta}^{\phi} + \frac{v}{a}\delta_\phi\bar{\theta}^{\lambda}\right)\right]^n \qquad (4.10)$$

$$r^{n+\frac{1}{2}} = \left[\bar{r}^{\lambda\phi} - \tfrac{1}{2}\Delta t \left(\frac{u}{a\cos\phi}\delta_\lambda \bar{r}^{\phi} + \frac{v}{a}\delta_\phi \bar{r}^{\lambda} \right) \right]^n \qquad (4.11)$$

$$u^{n+\frac{1}{2}} = \left[\bar{u}^{\lambda\phi} - \tfrac{1}{2}\Delta t \left(\frac{\bar{u}^{\lambda\phi}}{a\cos\phi}\delta_\lambda \bar{u}^{\phi} + \frac{\bar{v}^{\lambda\phi}}{a}\delta_\phi \bar{u}^{\lambda} \right) \right]^n \qquad (4.12)$$

$$v^{n+\frac{1}{2}} = \left[\bar{v}^{\lambda\phi} - \tfrac{1}{2}\Delta t \left(\frac{\bar{u}^{\lambda\phi}}{a\cos\phi}\delta_\lambda \bar{v}^{\phi} + \frac{\bar{v}^{\lambda\phi}}{a}\delta_\phi \bar{v}^{\lambda} \right) \right]^n \qquad (4.13)$$

In the second step we use fourth-order approximations to the derivatives:

$$\theta^{n+1} = \theta^n - \Delta t \left[\frac{u}{a\cos\phi} \left((1+c)\delta_\lambda \bar{\theta}^{\phi} - c\left(\tfrac{2}{3}\delta_{3\lambda}\bar{\theta}^{\phi} + \tfrac{1}{3}\delta_{3\lambda}\bar{\theta}^{3\phi} \right) \right) + \frac{v}{a} \left((1+c)\delta_\phi \bar{\theta}^{\lambda} - c\left(\tfrac{2}{3}\delta_{3\phi}\bar{\theta}^{\lambda} + \tfrac{1}{3}\delta_{3\phi}\bar{\theta}^{3\lambda} \right) \right) \right]^{n+\frac{1}{2}} \qquad (4.14)$$

$$r^{n+1} = r^n - \Delta t \left[\frac{u}{a\cos\phi} \left((1+c)\delta_\lambda \bar{r}^{\phi} - c\left(\tfrac{2}{3}\delta_{3\lambda}\bar{r}^{\phi} + \tfrac{1}{3}\delta_{3\lambda}\bar{r}^{3\phi} \right) \right) + \frac{v}{a} \left((1+c)\delta_\phi \bar{r}^{\lambda} - c\left(\tfrac{2}{3}\delta_{3\phi}\bar{r}^{\lambda} + \tfrac{1}{3}\delta_{3\phi}\bar{r}^{3\lambda} \right) \right) \right]^{n+\frac{1}{2}} \qquad (4.15)$$

$$u^{n+1} = u^n - \Delta t \left[\frac{\bar{u}^{\lambda\phi}}{a\cos\phi} \left((1+c)\delta_\lambda \bar{u}^{\phi} - c\left(\tfrac{2}{3}\delta_{3\lambda}\bar{u}^{\phi} + \tfrac{1}{3}\delta_{3\lambda}\bar{u}^{3\phi} \right) \right) + \frac{\bar{v}^{\lambda\phi}}{a} \left((1+c)\delta_\phi \bar{u}^{\lambda} - c\left(\tfrac{2}{3}\delta_{3\phi}\bar{u}^{\lambda} + \tfrac{1}{3}\delta_{3\phi}\bar{u}^{3\lambda} \right) \right) \right]^{n+\frac{1}{2}} \qquad (4.16)$$

$$v^{n+1} = v^n - \Delta t \left[\frac{\bar{u}^{\lambda\phi}}{a\cos\phi} \left((1+c)\delta_\lambda \bar{v}^{\phi} - c\left(\tfrac{2}{3}\delta_{3\lambda}\bar{v}^{\phi} + \tfrac{1}{3}\delta_{3\lambda}\bar{v}^{3\phi} \right) \right) \right.$$

$$+ \frac{v}{a}\left((1+c)\delta_\phi \bar{v}^{\lambda} - c\left(\frac{2}{3}\delta_{3\phi}\bar{v}^{\lambda} + \frac{1}{3}\delta_{3\phi}\bar{v}^{3\lambda}\right)\right)\Bigg]^{n+\frac{1}{2}} \qquad (4.17)$$

In equations (4.14) - (4.17), the parameter c is given by $c=\frac{3}{4}(1-\mu^2)$ where μ is the Courant number,

$$\mu = \left(\frac{u^2\Delta t^2}{a^2\cos^2\phi(\Delta\lambda)^2} + \frac{v^2\Delta t^2}{a^2(\Delta\phi)^2}\right)^{\frac{1}{2}} \qquad (4.18)$$

4.4 Horizontal diffusion.

The changes due to diffusion are calculated at timelevel n and added to the right-hand side of equations (4.14) -(4.17). Non-linear diffusion of the form $K|\nabla^2\chi|\nabla^2\chi$ is used, this being more scale selective than linear diffusion. In finite-difference form

$$\nabla^2\chi = \frac{1}{a^2\cos^2\phi}\delta_{\lambda\lambda}\chi + \frac{1}{a^2\cos\phi}\delta_\phi(\cos\phi\,\delta_\phi\chi) \qquad (4.19)$$

where χ = (θ , r, u or v).

Within the model's co-ordinate system, this horizontal diffusion operator is calculated on σ-surfaces. In regions of steep orography the σ-surfaces themselves slope steeply, and equation (4.19) does not provide an accurate representation of horizontal diffusion, since the atmosphere is strongly stratified in the vertical. This can lead to errors, particularly in the temperature fields. Above the boundary layer, equation (4.19) is modified to approximate horizontal diffusion on pressure surfaces by using the formula

$$\nabla_p^2\chi = \nabla_\sigma^2\chi - \frac{2\sigma}{p_*}\left[\frac{1}{a^2\cos^2\phi}\delta_\lambda(\delta_\sigma\bar{\chi}^{\sigma}\delta_\lambda p_*) + \frac{1}{a^2}\delta_\phi(\delta_\sigma\bar{\chi}^{\sigma}\delta_\phi p_*)\right] \qquad (4.20)$$

This includes a correction term for the local slope of the σ-surfaces.

5. LARGE-SCALE PRECIPITATION.

Large-scale or dynamic precipitation is produced when the air at model gridpoints becomes supersaturated as a result of convergence or radiative cooling. The parametrization scheme removes this excess moisture and allows it to fall as rain or snow. The effects of evaporation and the melting of snow on the falling precipitation are also taken into account.

5.1 The formation of precipitation through condensation.

Starting at the top of the model, the following calculation is performed for each level k in turn. First, the specific humidity, r_K, is compared with the saturation specific humidity, $r_S(T_K)$, corresponding to the temperature T_K at that gridpoint. (See Appendix C for details on the calculation of r_S). If $r_K \leq r_S(T_K)$, and there is no precipitation falling from higher levels, then we proceed to the next level below.

If $r_K > r_S(T_K)$, then the excess moisture is removed and the temperature is increased through the release of latent heat. Defining adjusted values of r_K and T_K by $r_S(T_K')$ and $T_K' = (T_K + \Delta T_K)$, we have

$$\Delta T_K = \frac{L_c}{c_p}\left(r_K - r_S(T_K')\right), \qquad (5.1)$$

where L_c is the latent heat of condensation and c_p is the specific heat of dry air at constant pressure. The adjustment is made so that the gridpoint is just saturated at the new temperature. On using the Clausius-Clapeyron relation, we have

$$r_S(T_K') = r_S(T_K) + \frac{\partial r_S}{\partial T}(T_K)\Delta T \doteq r_S(T_K)\left(1 + \frac{\varepsilon L_c \Delta T_K}{R\,T_K^2}\right) \qquad (5.2)$$

where ε is the ratio of the molecular weights of water and dry air. Equations (5.1) and (5.2) can be solved simultaneously for ΔT_K and $r_S(T_K')$ the new value of $r_S(T_K')$ being given by

$$r_s(T_K') = r_K' = r_K - \frac{[r_K - r_s(T_K)]}{[1 + (\varepsilon L_c^2 / c_p R)\, T_K^{-2}]} \qquad (5.3)$$

If the temperature is below freezing, the precipitation formed is assumed to freeze. A further contribution to the temperature increment is then derived from the the additional latent heat released using L_f, the latent heat of fusion.

The precipitation per unit mass resulting from the adjustment at this level, given by

$$P_K = r_K - r_s(T_K') , \qquad (5.4)$$

is added to any precipitation reaching this level from above.

5.2 Evaporation.

If $r_K < r_s(T_K)$, that is the air is not saturated at level k, and precipitation is falling from higher levels, a proportion is evaporated. The form of the evaporation is chosen to be consistent with the method employed in the deep convection scheme and is designed to give evaporation rates which are typically of the order of 7mm / day / 100mb. The evaporation per unit mass, E_K, is given by

$$E_K = \min \{ b(r_s(T_K) - r_K)\Delta t, P_K \} \qquad (5.5)$$

where $b = 2\times10^{-5}\ s^{-1}$, Δt is the timestep and P_K is the precipitation falling through the layer.

New values of r_K and T_K, say r_K'' and T_K'', as a result of the above evaporation are given by

$$r_K'' = r_K + E_K \quad \text{and} \quad T_K'' = T_K - L E_K / c_p ,$$

where L is the latent heat appropriate to the phase of the precipitation.

5.3 The melting of snow.

Snow is melted in the highest model layer whose temperature is greater than 273°K. All the precipitation falling into this layer is assumed to melt immediately. The accompanying change in temperature is therefore given by

$$\Delta T_K = -\frac{L_f}{c_p} \sum_{\ell=K+1}^{Top} (P_\ell - E_\ell) \, . \qquad (5.6)$$

A similar adjustment is made to the temperature field if the precipitation changes from rain to snow.

5.4 The precipitation reaching the surface.

From the above the amount of dynamic precipitation reaching the surface in one timestep, A_*, may be calculated. Expressed in mm per unit area

$$A_* = \frac{10^2}{g} P_* \sum_{\ell=1}^{Top} (P_\ell - E_\ell) \Delta\sigma_\ell \, . \qquad (5.7)$$

The rate of precipitation, R_*, in mm per hour is then given by

$$R_* = (3600 / \Delta t) A_* \, . \qquad (5.8)$$

6. DEEP-CONVECTION.

The deep-convection scheme, originally described by Lyne and Rowntree (1976), was developed using data from the GATE experiment for use in General Circulation studies. It is based on parcel theory modified by entrainment (Riehl 1954, Scorer 1958, Ludlam 1963) with a treatment of detrainment based on Ceselski (1972) and Arakawa (1969).

Several arbitrary parameters are encorporated within the scheme allowing adjustments to be made and the scheme to be "tuned". Many of these have been modified in the light of experience from the values originally quoted by Lyne and Rowntree. The values in current use in the operational model are shown in Table 6.1.

The bottom two levels of the operational model are combined for the purpose of convection. This avoids problems associated with the shallow nature of the bottom layer and is consistent with its treatment in the boundary layer scheme (Section 7). A convective adjustment step is performed as part of the boundary layer calculations in order to remove any instability between these layers.

6.1 The buoyancy equations.

The scheme assumes that in each grid box there is an ensemble of buoyant convective plumes with varying characteristics (temperature, humidity, cross-sectional area) which entrain air from the surrounding environment and ascend until they are no longer buoyant. Within the ensemble the virtual potential temperatures of the plumes are further assumed to be distributed about an average value

$$\left(\theta_v^p\right)_k = \theta_k^p\left(1 + 0.61\, r_k^p\right) \qquad (6.1)$$

Here r_k^p is the average specific humidity of the plumes with $r_k^p \leq r_s\left(\theta_k^p\right)$.

The finite difference treatment of the ensemble is best understood by reference to Figure 6.1. We define δ_K as the fractional rate of detrainment at level k and $\varepsilon_{K+\frac{1}{4}}$, $\varepsilon_{K+\frac{3}{4}}$ as the fractional entrainment rates at levels $k+\frac{1}{4}$, $k+\frac{3}{4}$. The entrainment rates are specified empirically within the model (see Table 6.1), whilst the detrainment rate is diagnosed by the convection scheme. The value of δ_K may be interpreted as the fraction of the ensemble whose plumes terminate at level k.

The vertical mass flux at level k, M_K, gives a measure of the size of the ensemble and is predicted by

$$M_{K+1} = \left(1+\varepsilon_{K+\frac{1}{4}}\right)\left(1+\varepsilon_{K+\frac{3}{4}}\right)\left(1-\delta_K\right) M_K . \qquad (6.2)$$

The treatment of the ensemble as it passes from level k to level k+1 is described by the following equations:

$$\left(1+\varepsilon_{K+\frac{1}{4}}\right)\left(1+\varepsilon_{K+\frac{3}{4}}\right)\left(1-\delta_K\right) r^P_{K+1} =$$
$$r^P_K - \delta_K r^R_K + \varepsilon_{K+\frac{1}{4}}\left(1-\delta_K\right) r^E_K + \varepsilon_{K+\frac{3}{4}}\left(1+\varepsilon_{K+\frac{1}{4}}\right)\left(1-\delta_K\right) r^E_{K+1} \qquad (6.3)$$

$$\left(1+\varepsilon_{K+\frac{1}{4}}\right)\left(1+\varepsilon_{K+\frac{3}{4}}\right)\left(1-\delta_K\right)\left[\theta^P_{K+1} - \frac{L}{c_p}\gamma_{K+1}\left(r^P_{K+1} - r_s(\theta^P_{K+1})\right)\sigma^{-K}_{K+1}\tilde{\Pi}^{-1}\right] =$$
$$\theta^P_K - \delta_K\theta^R_K + \varepsilon_{K+\frac{1}{4}}\left(1-\delta_K\right)\theta^E_K + \varepsilon_{K+\frac{3}{4}}\left(1+\varepsilon_{K+\frac{3}{4}}\right)\left(1-\delta_K\right)\theta^E_{K+1} \qquad (6.4)$$

where r^P_K is the specific humidity of the ensemble before condensation and $\gamma_K = 1$ if $r^P_K \geq r_s(\theta^P_K)$; otherwise $\gamma_K = 0$. A superscript E refers to environmental values whilst a superscipt R refers to detrainment values.

6.2 Detrainment.

Detrainment does not take place at the lowest convective level. Indeed at higher levels detrainment only takes place when it is necessary

to make the ensemble buoyant at the next level.

The ensemble is first raised from level k to level k+1 without detrainment. This is done by solving equations (6.3) and (6.4) with $\delta_K = 0$. The Clausius-Clapeyron relation is used to approximate $r_s(\theta^P_{K+1})$ in equation (6.4) by

$$r_s(\theta^P_{K+1}) = r_s(\theta^E_{K+1})\left[1 + \frac{L}{R_v}\frac{(\theta^P_{K+1} - \theta^E_{K+1})}{(T^E_{K+1})^2}\sigma^{kc}_{K+1}\tilde{\gamma}_{11}\right] \qquad (6.5)$$

If it is found that the virtual potential temperature of the ensemble is greater by a quantity b than that of the environmental air, that is

$$(\theta^P_v)_{K+1} - b > (\theta^E_v)_{K+1}, \qquad (6.6)$$

then the ensemble is assumed to be buoyant at this level and no detrainment occurs. The minimum excess buoyancy b allows for the spread of θ^P_v in the ensemble. Thus the characteristics of the ensemble at level k are now known.

If (6.6) is not satisfied, then it is assumed that sufficient detrainment has occured at level k at a virtual potential temperature of θ^E_v to raise the minimum θ_v of the plumes to that of the environment. Therefore defining the virtual potential temperature of detraining air by

$$(\theta^R_v)_K = \theta^R_K\left(1 + 0.61\gamma_K r_s(\theta^R_K) + 0.61(1-\gamma_K)r^P_K\right) \qquad (6.7)$$

we can set

$$(\theta^R_v)_K = (\theta^E_v)_K \qquad (6.8)$$

The potential temperature of detraining air may now be derived from equations (6.7) and (6.8) by using the Clausius-Clapeyron

relationship (see equation (6.5)) with the approximation

$$\theta^R_K \, r_s(\theta^R_K) = \theta^E_K \, r_s(\theta^R_K)$$

whence

$$\theta^R_K = \theta^E_K \left[1 + \frac{0.61 \left(r^E_K - r_s(\theta^E_K) \right)}{1 + 0.61 \, L/(R_v T^E_K) \, r_s(\theta^E_K)} \right] \qquad (6.9)$$

The detrainment rate δ_K may now be determined from equations (6.3) and (6.4) together with equation (6.9) by choosing a value for θ^P_{K+1} such that the ensemble is just buoyant; the buoyancy test (6.6) is treated in the same way as the derivation of equation (6.9) to give

$$\theta^P_{K+1} = \theta^E_{K+1} + \frac{0.61 \, \theta^E_{K+1} \left(r^E_{K+1} - r_s(\theta^E_{K+1}) \right) + b}{1 + 0.61 \, L/(R_v T^E_{K+1}) \, r_s(\theta^E_{K+1})} \qquad (6.10)$$

When dry convection is necessary, that is $\gamma_K = \gamma_{K+1} = 0$, this reduces to

$$\theta^P_{K+1} = \frac{\theta^E_{K+1} \left(1 + 0.61 \, r^E_{K+1} \right) + b}{1 + 0.61 \, r^P_{K+1}} \qquad (6.11)$$

6.3 Initiation of convection.

The model atmosphere is tested from the bottom upwards for convective instability by taking a parcel from level k to level k+1 with

$$\theta^P_K = \theta_I = \theta^E_K + S_\theta \quad \text{and} \quad r^P_K = r_I = r^E_K + S_r$$

where S_θ and S_r are constants. Convection is then initiated if the buoyancy test

$$(\theta^P_v)_{K+1} - (\theta^E_v)_{K+1} - b \geq E_{MIN} \, \Delta\sigma_{K+\frac{1}{2}} \qquad (6.12)$$

is satisfied. Here E_{MIN} is a constant and represents the minimum buoyancy required by the ensemble for convection to begin.

The initial mass flux ascribed to the ensemble is primarily based on the excess buoyancy and is given by

$$M_I = 10^{-3} \Delta t \left[d + c \left(\frac{(\theta_v^\rho)_{k+1} - (\theta_v^E)_{k+1} - b}{\Delta \sigma_{k+\frac{1}{2}}} \right) \right] \quad (6.13)$$

Here d and c are constants (see Table 6.1). The parameter d is designed to allow some convection to take place independently of the amount of excess buoyancy . M_I is additionally constrained to be smaller than the depth of the thinnest model layer to prevent over-stabilisation.

6.4 Termination of convection.

Convection continues upwards through the model atmosphere until the ensemble is no longer buoyant. This occurs when the upward mass flux becomes so small (less than a critical mass flux M_{MIN}) that the effects of convection would be negligible. Convection is therefore terminated when the residual mass flux

$$(1 - \delta_K) M_K < M_{MIN}, \quad (6.14)$$

with detrainment taking place at level k using the parcel values θ_K^ρ and r_K^ρ

Convection is also terminated at level k if an undilute parcel rising from the first convective layer (I) is stable in layer k+1. This happens when

$$(\theta_v^E)_{k+1} + b > \left(\theta_I^\rho + \frac{L}{c_p} \left(r_I^\rho - r_S(\theta_{k+1}^E) \right) \sigma_{k+1}^{-\kappa} \Pi^{-1} \right) \left(1 + 0.61\, r_S(\theta_{k+1}^E) \right) \quad (6.15)$$

This test prevents the detrainment from leading to excessive buoyancy.

6.5 Effects on the environment.

At those levels where convection has taken place the model's temperature and humidity fields are modified to take account of the changes in the nature of the environmental air. The latent heat released during condensation is added to the parcel temperature and so does not appear explicitly in the environmental heat budget. The changes described here are due to entrainment, detrainment and the subsidence which compensates for the parcel's upward mass flux. The effects of evaporation are considered in the next section.

For layer k the effects of the fluxes on the mass of the environmental air are

(i) Entrainment: a loss of

$$\left(\frac{\varepsilon_{k-\frac{1}{4}}}{1 + \varepsilon_{k-\frac{1}{4}}} + \varepsilon_{k+\frac{1}{4}} (1 - \delta_k) \right) M_k$$

at the environmental values of θ_k^E and r_k^E. In the lowest convective layer this transfer takes place with the values $\theta_k^E + S_\theta$ and $r_k^E + S_r$.

(ii) Detrainment: a gain of

$$\delta_k M_k$$

at the detrainment values of θ_k^R and $\gamma_k r_s(\theta_k^R) + (1 - \gamma_k) r_k^P$, except in the top layer where values of θ_k^P and r_k^P are used.

(iii) Downward mass flux into layer k: a gain of

$$(1 + \varepsilon_{k+\frac{1}{4}})(1 - \delta_k) M_k$$

at the environmental values of θ_{k+1}^E and r_{k+1}^E.

(iv) Downward mass flux out of layer k: a loss of

$$M_K \; / \; \left(1 + \varepsilon_{K+\frac{1}{4}} \right)$$

at the environmental values of θ^E_{K+1} and r^E_{K+1} . Note that this flux will be zero in the bottom convective layer.

On combining the effects (i) - (iv) the net change in the values of the environmental potential temperature and specific humidity at level k may be calculated. These are given by

$$\Delta\theta_K = \frac{M_K}{\Delta\sigma_K}\left[\left(1 + \varepsilon_{K+\frac{1}{4}}\left(1 - \delta_K \right)\right)\left(\theta^E_{K+1} - \theta^E_K\right) + \delta_K \left(\theta^R_K - \theta^E_{K+1}\right)\right] \qquad (6.16)$$

$$\Delta r_K = \frac{M_K}{\Delta\sigma_K}\left[\left(1 + \varepsilon_{K+\frac{1}{4}}\left(1 - \delta_K \right)\right)\left(r^E_{K+1} - r^E_K\right) + \delta_K \left(r^R_K - r^E_{K+1}\right)\right] \qquad (6.17)$$

6.6 Condensation, evaporation and precipitation.

The condensation, in mm per unit area, produced by taking the ensemble from level k to level k+1 is given by

$$P_K = \gamma_{K+1}\left(r^P_{K+1} - r_S\left(\theta^P_{K+1}\right)\right) M_{K+1}\left(\frac{10^2 p_*}{g}\right) \qquad (6.18)$$

This is assumed to be immediately converted into precipitation and is allowed to fall as snow or rain depending on the sign of

$$\frac{1}{2}\left(T^E_K + T^E_{K+1}\right) - 263$$

Here 263°K is assumed to be the temperature at which the effects of sublimation of water vapour into ice become pronounced. If $\gamma_{K+1} = 1$ the parcel humidity is then adjusted so that $r^P_{K+1} = r_S\left(\theta^P_{K+1}\right)$.

In order to allow for cloud dissipation and the effects of unsaturated downdraughts on the falling precipitation, some evaporation takes place at level k. This is done according to the formula

$$E_K = e\left(r_s(\theta_K^E) - r_K^E\right) M_{K+1}\left(\frac{10^2 p_* \Delta\sigma_K}{g}\right) \qquad (6.19)$$

where e is a constant. The evaporation is further constrained so that

$$E_K \leqslant P_K$$

The environmental temperature and humidity are then incremented by

$$\Delta r_K = \frac{g E_K}{p_* \Delta\sigma_K} \quad \text{and} \quad \Delta T_K = -\frac{L g E_K}{c_p p_* \Delta\sigma_K}$$

The falling precipitation changes state as it crosses the freezing level, and the model temperature fields are changed accordingly. (See Section 5.3).

The total convective precipitation reaching the surface may now be calculated from equations (6.17) and (6.18) by summing over the model levels in essentially the same way as in the large-scale precipitation scheme. (See Section 5.4).

6.7 Energy considerations.

The final stage of the scheme ensures that the vertically integrated sum of potential, internal and latent energies, that is

$$\int_0^1 \left(c_p T + L r\right) d\sigma , \qquad (6.20)$$

is conserved by the convective motions. The full environmental temperature increments are therefore adjusted so that

$$\sum_{K=1}^{Top} \left(c_p \Delta T_K + L \Delta r_K\right) \Delta\sigma_K = 0 \qquad (6.21)$$

by equalising the vertically integrated temperature increments of each sign.

Parameter	Meaning	Value
b	excess buoyancy of parcel for continuance of convection	0.2^{o} K
e	evaporation constant	4
$\varepsilon_{K+\frac{1}{4}}$	fractional entrainment rate at level $k+\frac{1}{4}$	$3\sigma_{K}(\sigma_{K}-\sigma_{K+\frac{1}{2}})$
$\varepsilon_{K+\frac{3}{4}}$	fractional entrainment rate at level $k+\frac{3}{4}$	$3\sigma_{K+\frac{1}{2}}(\sigma_{K+\frac{1}{2}}-\sigma_{K+1})$
c d	constants in initial mass flux formula	3.33×10^{-4} s^{-1} K^{-1} 0.0 s^{-1}
M_{MIN}	minimum mass flux	10^{-3} cΔt E_{MIN}
S_{θ} S_{r}	excess of initial parcel values over the environment	0.2^{o}K 0.0 Kg/Kg
E_{MIN}	Minimum parcel buoyancy	1^{o}K

Table 6.1 Values of adjustable parameters used in the operational deep convection scheme.

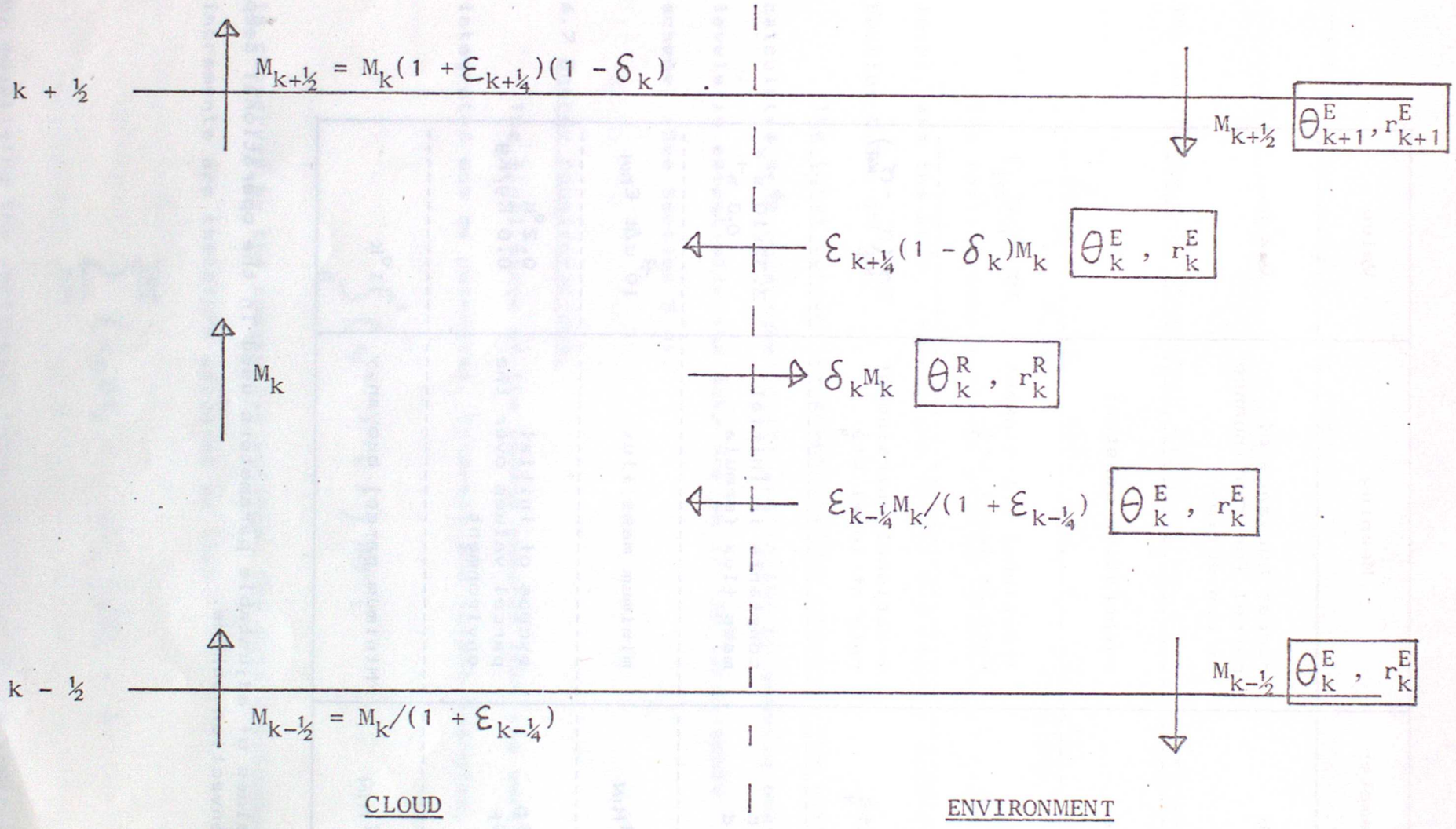

Figure 6.1. Vertical fluxes, entrainment and detrainment in the deep-convection scheme.

7. THE BOUNDARY LAYER.

The description of the transfer of heat, moisture and momentum through the earth's boundary layer by the process of vertical turbulent mixing is based on the scheme due to Richards (1980). The equations used are those for vertical diffusion with a variable eddy diffusion coefficient:

$$\frac{\partial u}{\partial t} = \frac{\partial}{\partial z}\left(K_M \frac{\partial u}{\partial z} \right) \qquad (7.1)$$

$$\frac{\partial v}{\partial t} = \frac{\partial}{\partial z}\left(K_M \frac{\partial v}{\partial z} \right) \qquad (7.2)$$

$$\frac{\partial r}{\partial t} = \frac{\partial}{\partial z}\left(K_H \frac{\partial r}{\partial z} \right) \qquad (7.3)$$

$$\frac{\partial \theta}{\partial t} = \frac{\partial}{\partial z}\left(K_H \frac{\partial \theta}{\partial z} \right) \qquad (7.4)$$

where K_M and K_H are the diffusion coefficients for momentum and heat respectively. Terms of the form $K\,\partial\chi/\partial z$ are referred to as the fluxes and are calculated at half-levels within the boundary layer. The problem of determining the effects of vertical exchanges within the boundary layer therefore reduces to that of specifying these fluxes. Note that the operational model has 4 full levels within its boundary layer, whilst for example the 11-level version has only 3 such levels.

7.1 Surface exchanges.

At the surface a drag coefficient approach is used, and these fluxes are given by the bulk aerodynamic formulae

$$F_u = - C_D |\underset{\sim}{V}_1| \, u_1 \qquad (7.5)$$

$$F_v = - C_D |\underset{\sim}{v}_1| \, v_1 \qquad (7.6)$$

$$F_\theta = - C_H |\underset{\sim}{v}_1| \, (\theta_1 - \theta_*) \qquad (7.7)$$

$$F_r = - C_H |\underset{\sim}{v}_1| \, (r_1 - r_s(\theta_*)) \qquad (7.8)$$

where $|\underset{\sim}{v}_1| = (u_1^2 + v_1^2)$.

In equations (7.5) - (7.8) the subscript 1 denotes values at the lowest model level, and * denotes surface values. Over land, θ_* is predicted in the model from a heat budget based on radiation, evaporation and sensible heat flux, whilst over the sea, it is held constant throughout a forecast.

The surface moisture fluxes are curtailed over dry surfaces, when the sign of F_r corresponds to evaporation into the atmosphere, by setting $F_r = 0$ at those model grid points designated as "arid" land. The model's surface land types are "snow-covered", "ice-covered", "temperate" and "arid". These are specified climatologically and are given in Appendix D.

The drag and exchange coefficients C_D and C_H depend on the roughness length z_0 (specified as 10^{-4} m over sea and 10^{-1} m over land) and the bulk Richardson number

$$(R_i)_B = \frac{g z_1}{\theta_1 |\underset{\sim}{v}_1|^2} \left[\theta_1 - \theta_* + 0.61 \, (r_1 - r_s(\theta_*)) \right] \qquad (7.9)$$

where z_1 is the height of the bottom level and $(r_1 - r_s(\theta_*))$ is treated in the same way as above. The form taken by C_D and C_H can be seen from Figures 7.1 and 7.2. Tabulated values of C_D and C_H are required near $(R_i)_B = 0$ (see Table 7.1). These are derived from Monin-Obukov similarity theory, which gives

$$C_H = \frac{k^2}{\int_{\zeta_0}^{\zeta} \psi_M(\zeta) \frac{d\zeta}{\zeta} \int_{\zeta_0}^{\zeta} \psi_H(\zeta) \frac{d\zeta}{\zeta}} \qquad (7.10)$$

$$C_D = \frac{k^2}{\left[\int_{\zeta_0}^{\zeta} \psi_M(\zeta) \frac{d\zeta}{\zeta} \right]^2} \qquad (7.11)$$

where $\zeta = z_1/L$, $\zeta_0 = z_0/L$, $K = 0.4$ is von-Karman's constant and L is the Monin-Obukov length

$$L = \left| \frac{c_D^{3/2}}{K \, c_H \, (R_i)_g} \right| z \qquad (7.12)$$

ψ_H and ψ_M are the Monin-Obukov similarity functions defined by

$$\frac{\partial \theta}{\partial z} = \frac{\theta_*}{Kz} \psi_H\left(\frac{z}{L}\right) \qquad (7.13)$$

$$\frac{\partial u}{\partial z} = \frac{u_*}{Kz} \psi_M\left(\frac{z}{L}\right) . \qquad (7.14)$$

The expressions used for ψ_H and ψ_M are

$$\psi_M = \psi_H = \begin{cases} (1 + 5\, z/L) & \text{for } z/L \leq 1 \\ 6 & \text{for } z/L > 1 \end{cases} \qquad (7.15)$$

in stable conditions (Webb, 1970), and

$$\psi_M = (1 + 15\, z/L)^{-0.275} \qquad (7.16)$$

$$\psi_H = (1 + 15\, z/L)^{-0.55} \qquad (7.17)$$

in unstable conditions (Dyer, 1967).

7.2 Vertical diffusion.

Within the remainder of the boundary layer, above the surface of the earth, the fluxes take the form

$$F_\chi = - K_\chi \frac{\partial \chi}{\partial z} \qquad (7.18)$$

where K_χ depends on the depth of the boundary layer z_b, the roughness length z_0, the stability R_i and the velocity gradient $|\partial \underset{\sim}{v} / \partial z|$ through a mixing length approach

$$K_\chi = l^2 f_\chi (R_i) \left| \frac{\partial \underset{\sim}{v}}{\partial z} \right| \qquad (7.19)$$

the local Richardson number being given by

$$R_i = \frac{g}{T} \frac{\partial \theta / \partial z}{|\partial \underset{\sim}{v} / \partial z|^2} . \qquad (7.20)$$

Note that in equation (7.20), the squared vertical shear in the denominator is computed as $|\delta_z \underset{\sim}{v}|^2/(\Delta z)^2$ and $|\delta_z \underset{\sim}{v}|_{K+\frac{1}{2}}$ is not allowed to fall below $.1/\Delta z_{K+\frac{1}{2}}$, where $\Delta z_{K+\frac{1}{2}} = z_{K+1} - z_K$.

The form chosen for the mixing length is

$$l = \left(\frac{1}{k z} + \frac{1}{l_A} \right)^{-1}, \qquad (7.21)$$

and is due to Blackadar (1975). Here z is the height of the half level at which K_χ is being calculated and k is von Karman's constant. l_A, the asymptotic mixing length, is given by

$$l_A = 0.089\, z_b, \qquad (7.22)$$

where z_b is the depth of the boundary layer in metres.

The form of the stability function $f_X(R_i)$ is based on that given by Hicks (1976) for $Ri > 0$, and Dyer and Hicks (1970) for $Ri \leq 0$:

$$f_u(R_i) = f_v(R_i) = \begin{cases} (1 - 16\,R_i)^{\frac{1}{2}} & \text{if} \quad R_i \leq 0 \\ (1 - 5\,R_i)^2 & \text{if} \quad 0 < R_i \leq 0.143 \\ \left(R_i^{-1} + 0.624\right) \times 9.546 \times 10^{-3} & \text{if} \quad 0.143 < R_i < 1.3183 \\ 0 & \text{if} \quad R_i \geq 1.3183 \end{cases} \qquad (7.23)$$

For fluxes of θ and r, the form of $f_X(R_i)$ is the same as in (7.23) except in the unstable case, where

$$f_\theta(R_i) = f_r(R_i) = (1 - 16\,R_i)^{\frac{3}{4}} \quad \text{if} \quad R_i \leq 0 \qquad (7.24)$$

Fluxes and hence K, $f(R_i)$ and R_i are calculated at model half-levels. The vertical finite differences used are therefore calculated between full levels.

The boundary layer depth, z_b, is defined to be the height of the lowest half level at which the vertical heat fluxes fall to zero, that is when $R_i \geq 1.3183$. The top of the boundary layer is not allowed to be higher than the half-level above the top full level in the boundary layer (the fourth level in the operational model).

7.3 Changes to the surface temperature.

The surface temperature changes are determined by the surface evaporation and the flux of sensible heat:

$$\frac{\partial T_*}{\partial t} = - \frac{c_H |v_1| \rho_*}{H} \left(c_p (\theta_* - \theta_1) - L(r_s(T_*) - r_1) \right) \qquad (7.25)$$

ρ_* is the density of air at the surface ($= p_* 10^2 / (R T_*)$ kg m), H is the thermal capacity of the soil and L is the appropriate latent heat for evaporation (including that of melting snow if $T_* \leq 273^\circ$). In addition, T_* is constrained to be $\leq 273.2^\circ$ over sea or land ice, and if $T_* \leq 271.2^\circ$ it is relaxed towards 271.2° over sea ice according to

$$\frac{\partial T_*}{\partial t} = 5 \times 10^{-6} (271.2 - T_*). \qquad (7.26)$$

See Appendix D for details on the specification of land-ice and sea-ice.

7.4 Stability considerations.

Equations (7.1) - (7.4) are solved in an explicit manner and it is necessary to limit the size of the fluxes given by the above scheme to the maximum allowable for computational stability. In atmospherically unstable conditions this constraint can lead to severe truncation of the surface fluxes when the bottom model layer is very thin, as is the case with the distribution of levels used in the operational model. A further step is therefore carried out which permits the proportion of the surface fluxes remaining beyond the maxima allowed for computational stability to be passed through the bottom level and attributed to the next level above.

A similar coupling of the bottom two layers of the model is also carried out in the deep convection scheme (see Section 6). A dry convective adjustment of these layers is therefore performed to remove any instability within them.

These steps may be summarised as follows:

(i) The vertical diffusion coefficient is limited by

$$K_\chi < (\Delta z_1 + \Delta z_2)(\Delta z_{1\frac{1}{2}})/2\Delta t$$

for the first half level and by

$$K_\chi < \Delta z_K \Delta z_{K+\frac{1}{2}} / 2\Delta t$$

for the Kth half level.

(ii) The bottom level fluxes are restricted by

$$|F_1| < \left| \frac{(\chi_1 - \chi_2)(\Delta z_1 + \Delta z_2)}{\Delta t} \right|$$

where Δz_1 and Δz_2 are the thicknesses of the 1st and 2nd layers.

(iii) The surface fluxes may be redistributed between the lowest two levels of the model. For any variable χ (= u, v, θ or r) if

$$|F_1| > \left| \frac{(\chi_1 - \chi_*)\Delta z}{\Delta t} \right| \quad \text{and} \quad (\chi_1 - \chi_*)(\chi_2 - \chi_*) > 0$$

then $F_1 - (\chi_1 - \chi_*)\Delta z_1 / \Delta t$ is added to F_2. If

$$|F_1| > \left| \frac{(\chi_1 - \chi_*)\Delta z_1}{\Delta t} \right| \quad \text{and} \quad (\chi_1 - \chi_*)(\chi_2 - \chi_*) < 0$$

then F_1 is reduced to $(\chi_1 - \chi_*)\Delta z_1 / \Delta t$.

If

$$|F_2| > \left| \frac{(\chi_2 - \chi_1)\Delta z_1}{\Delta t} \right| \quad \text{and} \quad (\chi_1 - \chi_2)(\chi_* - \chi_2) > 0$$

then $F_2 - (\chi_2 - \chi_1)\Delta z_1 / \Delta t$ is added to F_1. If

$$|F_2| > \left| \frac{(\chi_2 - \chi_1)\Delta z_1}{\Delta t} \right| \quad \text{and} \quad (\chi_1 - \chi_2)(\chi_* - \chi_2) < 0$$

then F_2 is reduced to $(\chi_2 - \chi_1)\Delta z_1 / \Delta t$.

(iv) The convective adjustment between the bottom two levels is applied when $\theta_1 > \theta_2$. All variables χ are mixed so that

$$\chi_1 = \chi_2 = \frac{\chi_1 \Delta\sigma_1 + \chi_2 \Delta\sigma_2}{\Delta\sigma_1 + \Delta\sigma_2}$$

where $\Delta\sigma_1$ and $\Delta\sigma_2$ are the thicknesses of the 1st and 2nd levels.

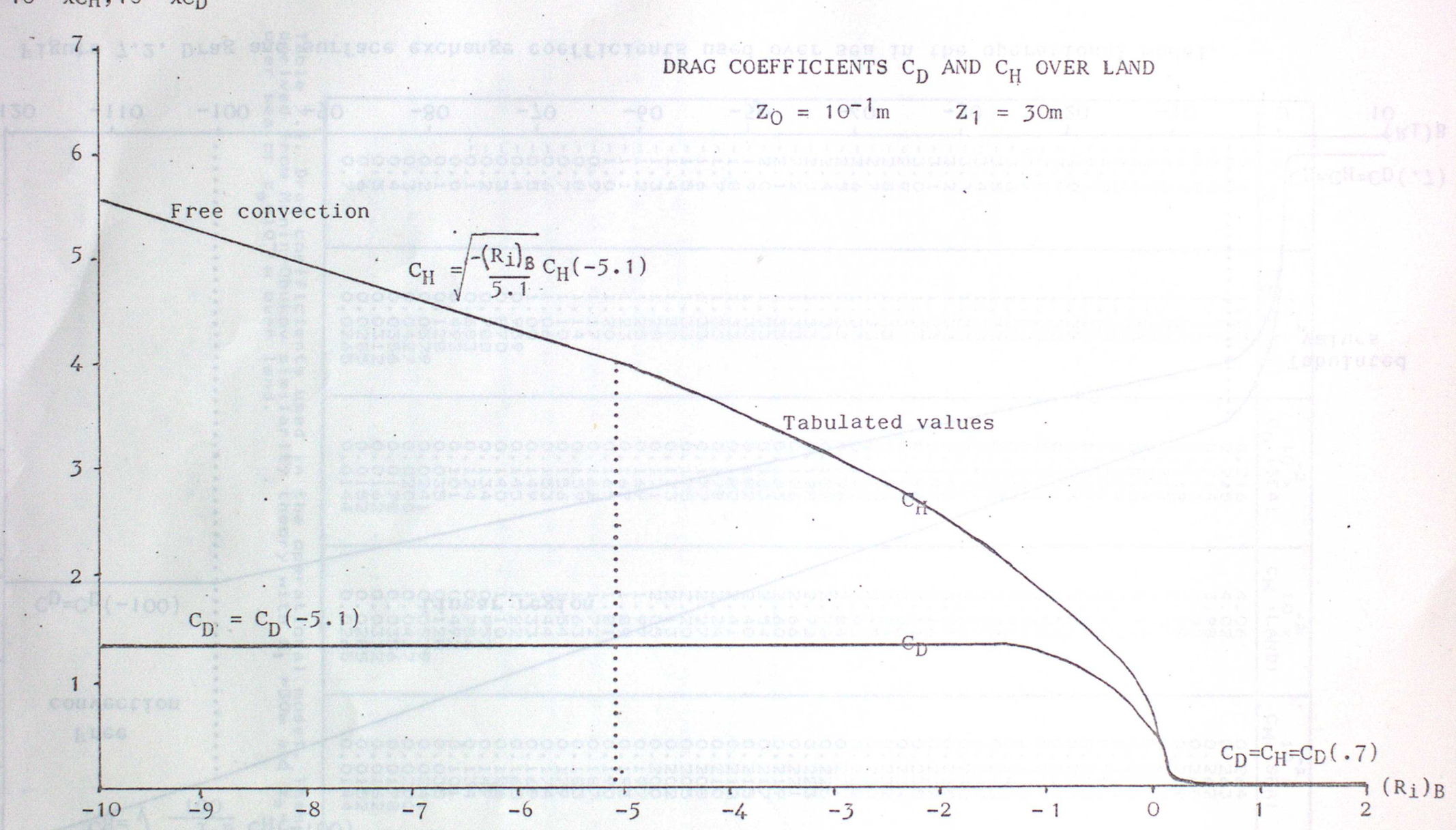

Figure 7.1. Drag and surface exchange coefficients used over land in the operational model.

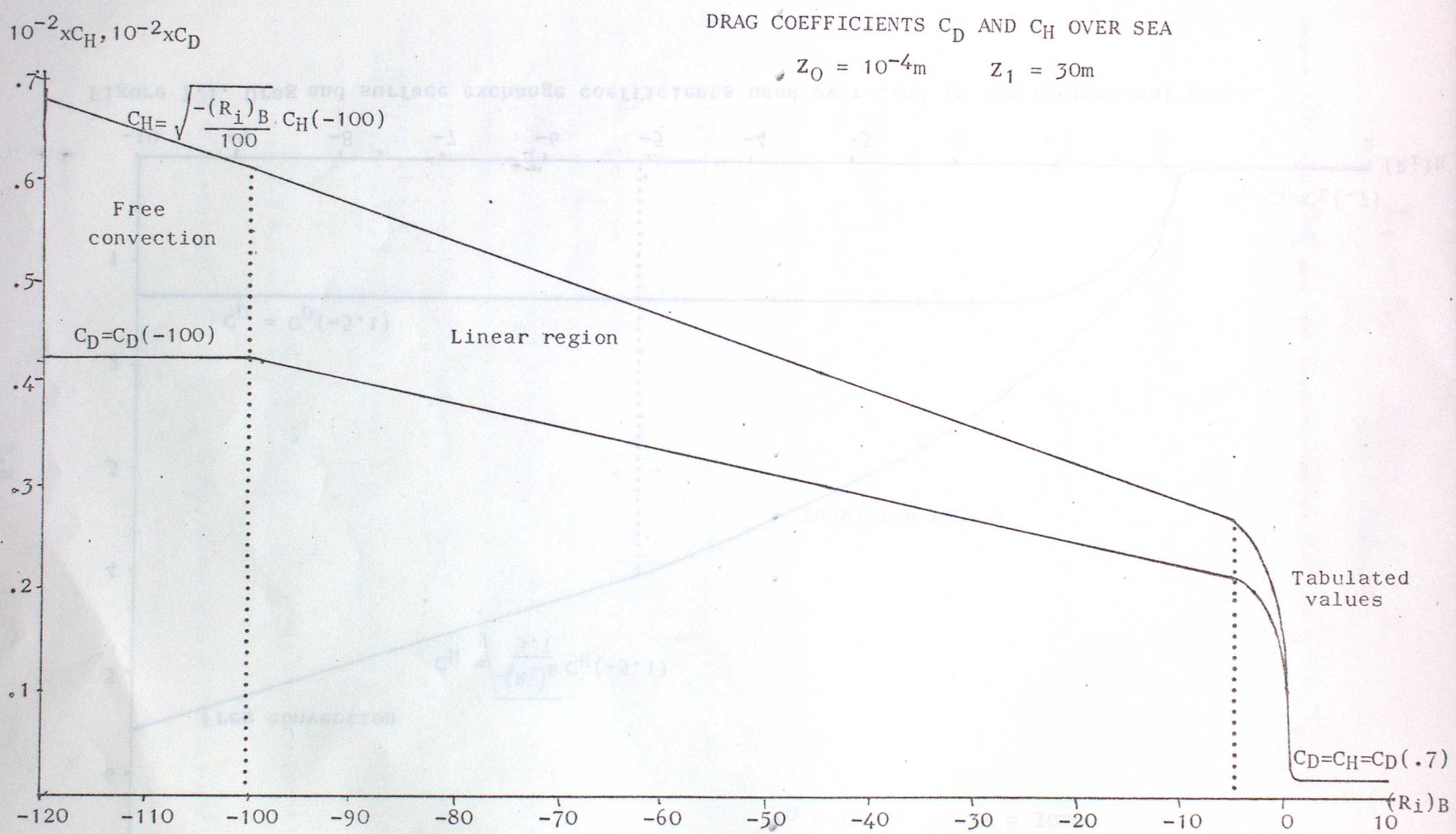

Figure 7.2. Drag and surface exchange coefficients used over sea in the operational model.

$(Ri)_B$	$10^{-2} \times C_D$ (LAND)	$10^{-2} \times C_D$ (SEA)	$10^{-2} \times C_H$ (LAND)	$10^{-2} \times C_H$ (SEA)
-5.1	1.33	0.216	4.06	0.264
-5.0	1.33	0.215	4.02	0.263
-4.9	1.33	0.214	3.98	0.262
-4.8	1.33	0.213	3.93	0.260
-4.7	1.33	0.212	3.89	0.259
-4.6	1.33	0.212	3.85	0.258
-4.5	1.33	0.211	3.81	0.257
-4.4	1.33	0.210	3.77	0.255
-4.3	1.33	0.209	3.72	0.254
-4.2	1.33	0.208	3.68	0.253
-4.1	1.33	0.207	3.64	0.252
-4.0	1.33	0.206	3.60	0.250
-3.9	1.33	0.206	3.55	0.249
-3.8	1.33	0.205	3.50	0.247
-3.7	1.33	0.204	3.46	0.246
-3.6	1.33	0.203	3.41	0.245
-3.5	1.33	0.202	3.36	0.243
-3.4	1.33	0.201	3.31	0.242
-3.3	1.33	0.199	3.26	0.240
-3.2	1.33	0.198	3.21	0.239
-3.1	1.33	0.197	3.16	0.237
-3.0	1.33	0.196	3.11	0.235
-2.9	1.33	0.195	3.06	0.234
-2.8	1.33	0.194	3.01	0.232
-2.7	1.33	0.193	2.95	0.230
-2.6	1.33	0.191	2.90	0.228
-2.5	1.33	0.190	2.84	0.227
-2.4	1.33	0.189	2.78	0.225
-2.3	1.33	0.188	2.72	0.223
-2.2	1.33	0.186	2.66	0.221
-2.1	1.33	0.185	2.60	0.219
-2.0	1.33	0.183	2.54	0.217
-1.9	1.33	0.182	2.48	0.215
-1.8	1.33	0.180	2.41	0.212
-1.7	1.33	0.179	2.34	0.210
-1.6	1.33	0.177	2.27	0.208
-1.5	1.33	0.175	2.20	0.205
-1.4	1.30	0.173	2.13	0.202
-1.3	1.28	0.171	2.05	0.200
-1.2	1.25	0.169	1.97	0.197
-1.1	1.23	0.167	1.89	0.193
-1.0	1.20	0.165	1.81	0.190
-0.9	1.17	0.162	1.72	0.187
-0.8	1.14	0.159	1.63	0.183
-0.7	1.10	0.156	1.54	0.179
-0.6	1.06	0.153	1.44	0.174
-0.5	1.00	0.149	1.33	0.169
-0.4	0.939	0.145	1.22	0.163
-0.3	0.870	0.140	1.10	0.156
-0.2	0.788	0.134	0.957	0.147
-0.1	0.683	0.124	0.786	0.134
0.0	0.492	0.101	0.492	0.101
0.1	0.128	0.035	0.128	0.035
0.2	0.0579	0.0241	0.0579	0.0241
0.3	0.0427	0.0200	0.0427	0.0200
0.4	0.0356	0.0178	0.0356	0.0178
0.5	0.0312	0.0162	0.0312	0.0162
0.6	0.0285	0.0152	0.0285	0.0152
0.7	0.0265	0.0144	0.0265	0.0144

Table 7.1. Drag coefficients used in the operational model. These are derived from Monin-Obukov similarity theory with z_1 =30m and $z_0=10^{-4}$ m over sea or $z_0=10^{-1}$ m over land.

8. RADIATION

The treatment of radiation in the model follows the ideas of Corby et al (1977) and Rowntree (1975). The scheme takes account of the seasonal and diurnal effects which influence the incoming solar radiation and longwave cooling to space, and modifies the model's temperature structure accordingly. The effects of cloud and humidity are not modelled directly but are inferred from zonally averaged climatological values. These climatological values specify the mean daily radiative heating and cooling rates and are kept constant throughout a forecast, normally at values appropriate to the initial time. This is acceptable for short-to-medium range forecasts but would be unsatisfactory for forecasts of an extended range. Appendix B tabulates the climatological functions used in the scheme.

This approach has led to a computationally economic scheme, often not the case with radiation parametrizations, whose performance in short-to-medium range forecasts compares favourably with schemes involving much more elaborate calculations.

It is possible to divide the scheme into four sections: solar heating of the atmosphere, solar heating at the surface, longwave cooling in the atmosphere and longwave cooling at the surface.

8.1 Long-wave cooling in the atmosphere.

The long-wave radiative cooling is calculated using empirical emissivities combined with the cooling to boundaries approximation to give cooling rates in the form

$$\frac{\partial T_K}{\partial t} = -a_K T_K^4 + b_K (T_*^4 - T_K^4) \qquad (8.1)$$

where T_K is the temperature of the Kth level and T_* is the surface

temperature. The parameters a_K and b_K are functions of latitude, pressure and time of year. Values of a_K are tabulated in Table B.5.

Since the second term on the righthand side of equation (8.1) is generally small, it is neglected outside the model's boundary layer. This term, in effect, represents the radiative exchange with the earth's surface. The coefficient b_K is assumed to be constant with height and is related to b_*, the coefficient of radiative exchange at the surface, by

$$b_K = \frac{g\, b_*}{c_p} \qquad (8.2)$$

The values of b_* used in the model are given in Table B.4.

8.2 Long-wave cooling at the surface.

From the parameter a_K, an effective emissivity ε_K for cooling to space may be calculated. This is given by

$$\varepsilon_K = \frac{a_K\, c_p\, p_* \,\Delta\sigma_K}{C\, g} \qquad (8.3)$$

where c_p is the specific heat of air and C is Stefan's constant. This allows the surface emissivity, ε_*, to be calculated from observed values of total column emissivity, ε_T, by using the relationship

$$\varepsilon_* = \varepsilon_T - \sum_{K=1}^{TOP} \varepsilon_K \qquad (8.4)$$

ε_T is tabulated in Table B.1.

The rate of long-wave cooling to space from the earth's surface may now be calculated using equation (8.4) and is given by

$$\frac{\partial T_*}{\partial t} = -\frac{C\, \varepsilon_* T_*^4}{H} \qquad (8.5)$$

where H is the thermal capacity of the soil, taken to be equivalent to that of 5cm of water.

A second term is also required in order to balance the heating of the bottom model layers through the radiative exchange term in equation (8.1). A compensating cooling of the ground is therefore encorporated through

$$\frac{\partial T_*}{\partial t} = -\frac{b_*}{H} \sum_{K=1}^{K=n_b} (T_*^4 - T_K^4) \qquad (8.6)$$

where b_* is the coefficient of radiative exchange at the surface and n_b is the number of model levels in the boundary layer.

8.3 Solar heating of the atmosphere.

The instantaneous solar heating rate, H_K, at level k is computed from the 24 hour mean value, $\overline{H}_K$, by imposing a diurnal variation such that

$$\frac{\partial T_K}{\partial t} = H_K = \beta \overline{H}_K \qquad (8.7)$$

where β depends on latitude, longitude, time of year and time of day. Values of $\overline{H}_K$ are given in Table B.6.

β is calculated by assuming that the solar radiation, R_K, reaching some point in the atmosphere at time t may be expressed as

$$R_K = F_K S \cos\xi \qquad (8.8)$$

where ξ is the zenith angle, S is the solar constant and F_K is an attenuation function that depends only on latitude, height and time of year.

The zenith angle may be expanded in terms of the model's parameters

so that equation (8.8) becomes

$$R_K = F_K S \left[\cos\phi \cos\delta \cos(\lambda+\tau) - \sin\phi \sin\delta\right] \qquad (8.9)$$

where δ is the solar declination, defined as being positive in the Northern Hemisphere. $\tau = t\pi/12$ and t is GMT in hours.

It is reasonable to assume that the instantaneous heating is proportional to the incident radiation. Thus

$$H_K = d R_K \qquad (8.10)$$

where d is a constant of proportionality. Moreover, $\overline{H_K}$ is similarly proportional to R_K integrated over the daylight hours. Therefore

$$\overline{H_K} = d \frac{F_K S}{2\pi} \int_{-\zeta-\lambda}^{\zeta-\lambda} \left[\cos\phi \cos\delta \cos(\lambda+\tau) - \sin\phi \sin\delta\right] d\tau$$

$$= d \frac{F_K S}{\pi} \left[\cos\phi \cos\delta \sin\zeta - \zeta \sin\phi \sin\delta\right] \qquad (8.11)$$

where ζ is half the length of daylight in radians given by

$$\cos\zeta = -\tan\phi \tan\delta$$

On substituting equations (8.10) and (8.11) into (8.7)

$$\beta = \begin{cases} \pi \dfrac{\left[\cos\phi \cos\delta \cos(\lambda+\tau) - \sin\phi \sin\delta\right]}{\left[\cos\phi \cos\delta \sin\zeta - \zeta \sin\phi \sin\delta\right]} & \text{if } |\tau| < \zeta \\ 0 \quad \text{if } |\tau| > \zeta \end{cases} \qquad (8.12)$$

8.4 Solar heating at the surface.

The surface solar heating is calculated in essentially the same way as the solar heating of the atmosphere, with allowances being made for the effects of the surface albedo, α . 24 hour mean values of the incident solar flux S_*, are used to give heating rates of the form

$$H_* = \frac{\beta S_{*(1-\alpha)}}{H} \qquad (8.13)$$

where β is given by equation (8.12) and H is the thermal capacity of the soil. Values of S_* are given in Table B.2.

The albedo is specified according to the values given in Table B.3, unless the suface is snow covered when α = 0.5 or ice covered when α = 0.8.

9. STABILITY AND ZONAL FILTERING.

A major problem with the regular latitude-longitude grid chosen for the model is that, due to the convergence of the meridians, the zonal separation of grid points decreases as the poles are approached. Thus, according to the Courant-Friedrichs-Lewy stability criterion (see Appendix A), a very short timestep is required in order to maintain computational stability at these high latitudes. For the global version of the model, for example, the adjustment timestep would need to be less than 18 seconds, making this model far too expensive to integrate.

An examination of the linear stability analysis presented in Appendix A shows that only certain wavelengths are unstable for a given gridlength and unstable timestep. This is manifested in an amplification rate greater than unity. Futhermore it is only those waves shorter than a critical gridlength that are unstable. The solution to our problem is therefore to keep a long timestep but remove or damp these short wavelengths by applying a zonal filter, therby increasing the effective zonal separation of the gridpoints without sacrificing the regularity of the grid.

The timestep is chosen to ensure that the model is both stable and economical, taking into account the computational expense of the zonal filter and any unacceptable loss in effective longitudinal resolution as the filtering region is extended equatorwards. An adjustment timestep of 5 minutes is used in the coarse-mesh model. This is stable within the region equatorwards of latitude 60°. The advection step of 15 minutes is also stable within this region provided that the maximum wind speed , U_{MAX}, is less than 116 m/s. (See Table 9.1).

9.1 Fourier filtering in the coarse-mesh model.

A Fourier chopping technique (Williamson, 1976) is used to zonally filter the global, 30°S and hemispheric versions of the forecast model,

and is applied to all prognostic variables at the end of each adjustment and advection step. Special measures are required for those variables that are strongly tied to the model orography since filtering along σ-surfaces will smooth some of the orographically induced variation. The scheme therefore filters the prognostic variables u, v and r together with Δp_* (the surface pressure increment) and a linear combination of θ and T, $\theta' = (\omega T + (1-\omega)\theta)$. The value of ω varies with height allowing a gradual change from θ near the ground to T at upper levels. ω is tabulated in Table 9.2,

Note that increment filtering could be used, as is done in the fine mesh model, but the above procedure is prefered for reasons of computational economy.

The linear stability criteria (A.20) and (A.24) are combined in the model for the purposes of Fourier chopping. It is easily shown that for any latitude, ϕ, the model is computationally stable at zonal wavenumber, j, provided that

$$a \cos\phi \Delta\lambda \geq B \sin\frac{\pi j}{N}, \qquad (9.1)$$

where $B = c\delta t$ in the case of the adjustment step and $B = U_{MAX}\Delta t$ in the case of the advection step. N is the number of points around a latitude circle and c is the phase speed of the external gravity wave.

The filter is applied polewards of a predetermined latitude, $\tilde{\phi}$, where the condition

$$a \cos\tilde{\phi} \Delta\lambda \geq B \qquad (9.2)$$

holds for both the adjustment and advection steps. $\tilde{\phi}$ would normally be the latitude at which condition (9.2) is just satisfied. For each latitude $\phi > \tilde{\phi}$ a maximum wave number j' may now be found from conditions (9.1) and

(9.2) such that

$$\sin \frac{\pi j'}{N} \leqslant \frac{\cos \phi}{\cos \tilde{\phi}} \qquad (9.3)$$

and stability is ensured for all $j \leqslant j'$.

Zonal Fourier coefficients are obtained by applying the discrete Fourier Transform:

$$\hat{\chi}_j(\phi, \sigma) = \frac{1}{N} \sum_{\ell=0}^{N-1} \chi(\lambda_\ell, \phi, \sigma)\, e^{-ij\lambda_\ell} \qquad (9.4)$$

where $\phi > \tilde{\phi}$, $-N/2 < j < N/2+1$, $\lambda_\ell = 2\pi\ell/N$ and $\chi = (u, v, r, \Delta p_x \text{ or } \theta)$.

The high wavenumber coefficients, that is $|j| > j'$, are then set to zero, and the filtered field χ' is constructed using

$$\chi'(\lambda_\ell, \phi, \sigma) = \sum_{j=-j'}^{j=j'} \hat{\chi}_j(\phi, \sigma)\, e^{i\ell\lambda_j} \qquad (9.5)$$

Note that the use of discrete Fourier Transforms to perform the above filtering is only possible because of the high computational speeds provided by the special implementation of the Fast Fourier Transform algorithms on the Cyber 205 computer (Temperton, 1982).

9.2 Multipoint filtering in the fine-mesh model.

The zonal periodicity required for the direct application of the Fourier Transform is not present in the fine-mesh model because of the restricted nature of its forecast domain. An alternative method to the one described above must therefore be sought.

The chosen approach uses a multipoint filtering technique based on the ideas of Hills (1982). A local approximation to the Fourier Transform is used to construct a filter of the form

$$\Delta\chi'_{\ell} = \sum_{m=-M}^{m=M} c_m \Delta\chi_{\ell+m}, \qquad (9.6)$$

where M is the half width of the filter and $\Delta\chi$ = (Δ u, Δ v, Δ p_x, Δ r or $\Delta\theta$). A value of M = 12 is used in the operational model.

The coefficients $c_{-M}, \ldots\ldots\ldots, c_M$ are constants for a given latitude and are calculated from the amount of damping required for linear stability. This method is therefore equivalent to reducing the amplitude of each wave by the amount of unstable amplification. The increments are assumed to be zero outside the east-west lateral boundaries of the model so that the filter may be applied near the edges of the forecast area.

The coefficients $c_{-M}, \ldots\ldots\ldots, c_M$ are determined by taking an Inverse Fourier Transform of the form

$$c_m = \frac{1}{N} \sum_{j=-\frac{N}{2}}^{j=\frac{N}{2}+1} \frac{1}{\bar{A}(\lambda_j)} e^{im\lambda_j} \qquad (9.7)$$

where $|m| \leq M$, N is the number of points around a latitude circle, using the zonal grid separation of the fine mesh model, and $\bar{A}$ is an amplification factor predicted by linear theory. The values produced by solving equation (9.7) are then adjusted so that

$$\sum_{m=-M}^{m=M} c_m = 1 \qquad (9.8)$$

in order that the mean value along a row is conserved by the filter.

The form of the amplification factor, $\bar{A}$, is provided by the linear analysis presented in Appendix A. From equation (A.16)

$$\bar{A}_{ADJ}(\lambda_j) = 2\mu^2 \sin^2\frac{\lambda_j}{2} - 1 + 2\left(\mu^2 \sin^2\frac{\lambda_j}{2} - \mu \sin\frac{\lambda_j}{2}\right) \qquad (9.9)$$

with $\mu^2 = \dfrac{B^2}{a^2 \Delta\lambda^2 \cos^2\phi}$, $B^2 = \gamma^2 c^2 \delta t^2$ and $\gamma^2 \geq 1$,

and from equation (A.23)

$$A_{ADV}(\lambda_j) = 1 - 4\mu^2(1-\mu^2)^2\left[1 + (1-\mu^2)\sin^2\frac{\lambda_j}{2}\right]\sin^4\frac{\lambda_j}{2} \quad (9.10)$$

with $B^2 = \gamma^2 U_{MAX}^2 \Delta t^2$ and $\gamma^2 \geq 1$.

On combining equations (9.9) and (9.10), $\bar{A}$ is defined by

$$\bar{A}(\lambda_j) = \text{MAX}\left(A_{ADJ}(\lambda_j), A_{ADV}(\lambda_j), 1\right)$$

γ is a constant and allows for the approximate modelling of the response (9.7) caused by the truncation of the Fourier series. At present a value of $\gamma = 1.2$ is used.

LAT (°) / Δt (MINS)	45	60	80
10	246	174	60
15	164	116	40
20	123	87	30

Table 9.1. The maximum stable wind speed predicted by linear theory for the advection step of the coarse mesh model.

Level	ω
10 - 15	1
5 - 10	0.5
1 - 4	0

Table 9.2. The weighting coefficient used for calculating the filtered field, $\theta' = (\omega T + (1 - \omega)\theta)$.

10. LATERAL BOUNDARY CONDITIONS AND THE TREATMENT OF THE POLES.

10.1 Fine-mesh model.

In the fine-mesh model, which covers a restricted geographical area, the boundaries can influence the synoptic behaviour over the whole forecast region in a short time. It is therefore necessary to impose boundary conditions which allow the movement of synoptic features through the edges of the forecast region.

This is done by extracting values of the prognostic variables p_*, θ, r, u and v from a coarse mesh forecast at hourly intervals and linearly interpolating these to the corresponding fine-mesh boundary points. These are then converted into tendencies. The fine-mesh boundaries are updated using these tendencies every advection timestep. Thus, for any variable χ (= u, v, θ, r or p_*)

$$\chi_b^{n+1} = \chi_b^n + \Delta t \left(\frac{\partial \chi_b}{\partial t}\right)_c^n \qquad (10.1)$$

where suffix b refers to boundary values and suffix c refers to values interpolated from the coarse mesh model.

A region of high diffusion is imposed around the edges of the fine-mesh area to smooth any roughnesses caused by inconsistencies between the fine-mesh and coarse-mesh forecasts. The diffusion coefficient used in this zone is currently set at three times the value used in the interior of the forecast region.

10.2 The treatment of the poles.

In coarse-mesh forecasts the variables p_*, θ and r are stored at the poles but not predicted independently; at each timestep their values are set equal to the mean of the surrounding points. Thus, for example, when computing the value of the surface pressure at the poles, p_*^P, it is

given by

$$p^{P}_{*} = \frac{1}{N}\sum_{\ell=1}^{N} p^{A}_{*\ell} \qquad (10.2)$$

where N is the number of model points in the east-west direction and the superscript A refers to the values on the row adjacent to the pole.

The above procedure cannot be directly applied to the polar values of the wind field (u^P, v^P), since they are stored at the half grid positions. Instead a mean cartesian wind is first calculated at the pole and this is then used to compute new values of (u^P, v^P). Hence at the North Pole for m = 1, ... , N

$$u_m = \frac{1}{N}\sum_{\ell=1}^{N}(u^A_\ell \cos\gamma_\ell - v^A_\ell \sin\gamma_\ell)\cos\gamma_m + \frac{1}{N}\sum_{\ell=1}^{N}(u^A_\ell \cos\gamma_\ell + v^A_\ell \sin\gamma_\ell)\sin\gamma_m$$

$$v_m = \frac{1}{N}\sum_{\ell=1}^{N}(u^A_\ell \cos\gamma_\ell + v^A_\ell \sin\gamma_\ell)\cos\gamma_m - \frac{1}{N}\sum_{\ell=1}^{N}(u^A_\ell \cos\gamma_\ell - v^A_\ell \sin\gamma_\ell)\sin\gamma_m \qquad (10.3)$$

where superscipt A again refers to the row adjacent to the polar row and $\gamma_m = 2\pi m / N$.

10.3 The southern boundary in hemispheric and 30°S forecasts.

The values of the prognostic variables are kept constant along the southern boundary during hemispheric and 30°S forecasts. The mean meridional velocity at the southern boundary is constrained to be zero by initially setting

$$v'_m = v_m - \frac{1}{N}\sum_{\ell=1}^{N} v_\ell$$

for m= 1, ... , N . This ensures that there is no net mass flow through the boundaries.

REFERENCES.

Arakawa,A.	1966	Computational Design for Long-Term Numerical Integrations of the Equations of Atmospheric Motion. J. Comput. Phys., 1, pp. 119-143.
Arakawa,A.	1969	Parametrization of Cumulus Convection. Proc. WMO/IUGG Symposium on Numerical Weather Prediction, Tokyo, Japan Met Agency, Tech. Report 67, pp IV-8-1 to IV-8-6.
Blackadar,A.K.	1975	High Resolution Models of the Planetary Boundary Layer. EPA-SRG Annual Report 1975, Contribution from Pennsylvania State University.
Burridge,D.M. and Gadd,A.J.	1977	The Meteorological Office Operational 10-level Numerical Weather Prediction Model (December 1975). Meteorological Office Scientific Paper No. 34, London, HMSO.
Ceselski,B.F.	1972	A Comparison of Cumulus Parametrization Techniques in Numerical Integrations of an Easterly Wave, Report 4 in Numerical weather prediction over the tropics. Report No. 72-1, Dept. Met., Florida State University, Tallahassee.
Corby,G.A., Gilchrist,A. and Rowntree,P.R.	1977	United Kingdom Meteorological Office Five-Level General Circulation Model. Methods in Comp. Phys., 17, pp. 67-166.
Cullen,M.J.P., Foreman,S.J., Prince,J.W., Radford,A.M. and Roskilly,D.R.	1981	Forecast Intercomparisons of Three Numerical Weather Prediction Models from the United Kingdom Meteorological Office. J. Atmos. Sci., 109, pp. 422-452.
Dyer,A.J.	1967	The Turbulent Transport of Heat and Water Vapour in an Unstable Atmosphere. Q. J. R. Met. Soc., 93, pp. 501-508.
Dyer,A.J. and Hicks,B.B,	1970	Flux-Gradient Relationships in the Constant Flux Layer. Q. J. R. Met. Soc., 96, pp. 715-721.
Gadd,A.J.	1978a	A Split Explicit Integration Scheme for Numerical Weather Prediction. Quart. J. R. Met. Soc., 104, pp. 569-582.
Gadd,A.J.	1978b	A Numerical Advection Scheme with Snmall Phase Errors. Quart J. R. Met. Soc., 104, pp. 583-594.
Gadd,A.J.	1980	Two Refinements to the Split Explicit Integration Scheme. Quart. J. R. Met. Soc., 106, pp. 215-220.

Hicks,B.B.	1976	Wind Profile Relationships from the "Wangara" Experiment. Q. J. R. Met. Soc., 102, pp. 535-551.
Hills,T.S.	1982	The Use of a Numerical Filter to Control Stability in a General Circulation Model. Met O 20 Tech. Note II/179, U.K. Meteorological Office, Bracknell.
Janic,Z.I.	1979	The Forward-Backward Scheme Modified to Prevent Two-Grid Interval Noise and its Application in σ-Coordinate Models. Cont. to Atmos. Physics., 52, p. 69.
Lyne,W.H. and Rowntree,P.R.	1976	Development of a Convective Parametrization Using GATE Data. Met O 20 Tech. Note II/70, Meteorological Office, Bracknell.
Lyne,W.H., Little,C.T., Dumelow,R.K. and Bell,R.S.	1983	The Operational Data Assimilation Scheme. Met O 11 Tech. Note No. 168, Meteorological Office, Bracknell.
Ludlam,F.H.	1963	Severe Local Storms - A Review. Meteorological Monographs, 5, pp. 1-30, Amer. Met. Soc..
Mesinger,F.	1973	A Method for Construction of Second-Order Accuracy Difference Schemes Permitting No False Two-Grid Interval Wave in the Height Field. Tellus, 25, pp. 444-458.
Monin,A.S. and Obukov,A.M.	1954	Basic Laws of Turbulent Mixing in the Ground Layer of the Atmosphere. Akad. Nauk. SSSR Geofiz. Inst. Tr., 151, pp. 163-187.
Phillips,N.A.	1957	A Coordinate System Having Some Special Advantages for Numerical Forecasting. J. Meteor., 14, pp. 184-185.
Richards,P.J.R.	1977	A Comparison of an Interactive Radiation Scheme and One Based on Climatology for Use in the High-Resolution Model. Met O 20 Tech. Note II/98, Meteorological Office, Bracknell.
Richards,P.J.R.	1980	The Parametrization of Boundary Layer Processe in General Circulation Models. PhD Thesis, University of Reading, U.K..
Riehl,H.	1954	Tropical Meteorology. Mc Graw-Hill, New York.
Rowntree,P.R.	1973	Proposed Convection Scheme for the 11-layer Tropical Model. Internal typescript, Met O 20, U.K. Meteorological Office, Bracknell.
Rownt[illegible]P.R.	1975	The Representation of Radiation and Surface Heat Exchange in a General Circulation Model. Met O 20 Tech. Note II/58, U.K. Meteorological Office, Bracknell.

Saker,N.J.	1975	An 11-Layer General Circulation Model. Met O 20 Tech. Note II/30, Meteorological Office, Bracknell.
Scorer,R.S.	1958	Natural Aerodynamics, Pergamon Press, London.
Williamson,D.L.	1976	Linear Stability of Finite-Difference Approximations on a Uniform Latitude-Longitude Grid with Fourier Filtering. Monthly Weather Review, 104, pp. 31-41.
Webb,E.K.	1970	Profile Relationships: The Log-Linear Range, and Extension to Strong Stability. Q. J. R. Met. Soc., 96, pp. 67-90.

NOTATION

Independent variables.

λ .....longitude

ϕ .....latitude

$\sigma = p/p^*$.....vertical coordinate

t.....time

Dependent variables.

θ .....potential temperature.....($^\circ$K)

p^*.....surface pressure.....(mb)

r.....specific humidity.....(Kg/Kg)

T^*.....surface temperature.....($^\circ$K)

u.....zonal wind component.....(ms^{-1})

v.....meridional wind component.....(ms^{-1})

Diagnostic variables.

$\Phi = gz$.....geopotential height.....($m^2 s^{-2}$)

$\dot{\sigma}$ .....vertical velocity.....(s^{-1})

$\theta_v = \theta(1+0.61r)$....vitual potential temperature.....($^\circ$K)

$p = \sigma p^*$.....pressure.....(mb)

$T = \theta(p/1000)^\kappa$.....temperature.....($^\circ$K)

$T_v = T(1+0.61r)$.....virtual temperature.....($^\circ$K)

$\Pi = (P^*/1000)^\kappa$.....Exner function

r_s .....saturation specific humidity.....(Kg/Kg)

z.....height.....(m)

Indices.

*.....suffix indicating surface value

k.....index indicating a model level

n.....index indicating time level

s.....suffix indicating saturation value

Constants and parameters.

a.....radius of the Earth.....($6.3712\ 10^{6}$ m)

a_K.....longwave cooling coefficient at level k

b_K, b*.....radiative exchange coefficient at level k and at the surface

c_p.....specific heat capacity for dry air at constant pressure.....($1004.8\ JKg^{-1}K^{-1}$)

$f = 2\Omega \sin\phi$.....Coriolis parameter [$\Omega = 2\pi/86400\ s^{-1}$]

f_X.....stability function used in definition of vertical diffusion coefficients

g.....acceleration due to gravity.....($9.81\ ms^{-2}$)

k.....von Karman's constant.....(0.4)

l, l_A.....mixing length and asymptotic mixing length

z_o.....roughness length.....(sea=10^{-4} ; land=10^{-1}

C.....Stephan's constant.....($5.6698\ 10^{-8}\ Js^{-1}m^{-2}K^{-4}$)

C_D, C_H.....drag coefficient and exchange coefficient for sensible and latent heat

E_K.....evaporation per unit mass of air at level k

E_{MIN}.....minimum convective parcel buoyancy

F.....Coriolis term in λ-ϕ coordinates [f + u tanϕ/a]

F_u, F_V, F_θ, F_r.....vertical fluxes of momentum, heat and moisture

$\mathbb{F}_u$, $\mathbb{F}_V$, $\mathbb{F}_\theta$, $\mathbb{F}_r$.....sources and sinks of momentum, heat and moisture

H.....thermal capacity of soil.....($2.0833\ 10^{4}\ JK^{-1}$)

$\overline{H}$, $\mathcal{H}$.....mean and instantaneous solar heating rates

K_χ.....diffusion coefficient for variable χ

L_c.....latent heat of condensation.....($2.3889\ 10^{6}\ JKg^{-1}$)

L_f.....latent heat of fusion of ice.....($3.3352\ 10^{5}\ JKg^{-1}$)

L.....latent heat of condensation or sublimation depending on the temperature

L_4.....Monin-Obukov length scale

M_I, M_{MIN}, M_K.....initial, minimum and level k values of vertical mass flux in convective plume

N.....number of grid points around a latitude circle

P_K.....precipitation per unit mass of air at level k

R.....gas constant for dry air.....(287.04 $JKg^{-1}K^{-1}$)

R_V.....gas constant for water vapour.....(461.51 $JKg^{-1}K^{-1}$)

Ri.....local Richardson number

$(Ri)_B$.....bulk Richardson number

S_*.....incident solar flux at the ground

α.....albedo

δ.....solar declination

δ_K.....fractional detrainment rate at level k

δ_λ, δ_ϕ.....finite difference operators

δt, Δt.....adjustment, advection timesteps

ε.....ratio of molecular weights of water and dry air.....(0.622)

$\varepsilon_{K+\frac{1}{4}}$, $\varepsilon_{K+\frac{3}{4}}$.....fractional entrainment rates

ε_T, ε_*, ε_K.....total, surface and level k emissivities

$\kappa = R/c_p$.....power used in Exner function

μ, ν.....Courant numbers

ψ_M, ψ_H.....Monin-Obukov similarity functions

τ.....GMT in hours

χ.....u, v, θ, r or p* depending on context

Φ_*.....geopotential height of orography

APPENDIX A.

A linear stability analysis

A.1 Introduction.

This section considers some of the stability properties of the operational integration scheme which can be inferred from analysing simple linearised forms of the equations of motion.

Gadd (1978a) has shown that for the version of the scheme used in the 10-level model, a sufficient condition for computational stability is (i) for the advection step

$$U\Delta t/\Delta \leqslant 1 \qquad (A.1)$$

where U is the maximum wind speed, Δt is the advection timestep and Δ is the gridlength, and

(ii) for the adjustment step

$$c\,\delta t/\Delta \leqslant 1 \qquad (A.2)$$

where c ($\approx$300 m/s) is the phase speed of the fastest moving gravity wave, δt is the adjustment timestep and Δ is the gridlength.

These results, whose general form is known as the Courants-Friedrichs-Lewy (C.F.L) stability criterion, allow a choice of timestep and gridlength which ensure a stable integration. In practice, because the operational model uses a latitude-longitude grid, conditions (A.1) and (A.2) are not satisfied near the poles and more detailed information about the behaviour of the scheme is required in order to implement the Fourier filtering which damps the unstable zonal wavenumbers at high latitudes.

A.2 The adjustment step.

When the gravity-inertia terms in the continuous equations of

motion are linearised they may be expressed as the set of two-dimensional gravity wave equations

$$\frac{\partial u}{\partial t} + g\frac{\partial h}{\partial x} = 0 \qquad \text{(A.3)}$$

$$\frac{\partial v}{\partial t} + g\frac{\partial h}{\partial y} = 0 \qquad \text{(A.4)}$$

$$\frac{\partial h}{\partial t} + H\left(\frac{\partial u}{\partial x} + \frac{\partial v}{\partial y}\right) = 0 \qquad \text{(A.5)}$$

where H is the equivalent depth of the linearised atmosphere and g is the acceleration due to gravity. For convenience a cartesian grid is assumed with h representing height. Note that the gravity wave propagation speed is given by $c = (gH)^{\frac{1}{2}}$.

The details of the forward-backward scheme used in the adjustment step of the forecast model are presented in Section 4.2. If this scheme is applied to equations (A.3) - (A.5), the following set of difference equations is obtained:

$$u^{n+1} = u^{n} - g\,\delta t\,\delta_x \bar{h}^{y\,n+1} \qquad \text{(A.6)}$$

$$v^{n+1} = v^{n} - g\,\delta t\,\delta_y \bar{h}^{x\,n+1} \qquad \text{(A.7)}$$

$$h^{n+1} = h^{n} - H\,\delta t\,(\delta_x \bar{u}^{y} + \delta_y \bar{v}^{x\,n}) + wgH\,\delta t^2(\nabla_t^2 - \nabla_x^2)h^{n} \qquad \text{(A.8)}$$

where the same notation is used as in Section 4.

The stability properties of these equations may be investigated by considering Fourier modes of the form

$$u^{n} = u_0\,\xi^{n}\,e^{i(jx+\ell y)}, \quad v^{n} = v_0\,\xi^{n}\,e^{i(jx+\ell y)} \quad \text{and} \quad h^{n} = h_0\,\xi^{n}\,e^{i(jx+\ell y)}$$

where j and ℓ are wave numbers in the x and y directions respectively. This means that, for example, $u^{n} = \xi\, u^{n-1}$ and $|\xi|$ is therefore the amount that each Fourier mode is damped or amplified in one timestep. If $|\xi| > 1$,

then the scheme is computationally unstable. Equations (A.6) - (A.8) may now be written as

$$(\xi - 1)u_o + 2ig\xi\frac{\delta t}{\Delta x} h_o \sin\alpha\cos\beta = 0 \qquad (A.9)$$

$$(\xi - 1)v_o + 2ig\xi\frac{\delta t}{\Delta y} h_o \sin\beta\cos\alpha = 0 \qquad (A.10)$$

$$2i\xi H\delta t\left(\frac{u_o}{\Delta x}\sin\alpha\cos\beta + \frac{v_o}{\Delta y}\sin\beta\cos\alpha\right) +$$

$$\left[\xi - 1 + 4wgH\delta t^2\left(\frac{1}{\Delta x^2} + \frac{1}{\Delta y^2}\right)\sin^2\alpha\sin^2\beta\right] h_o = 0 \qquad (A.11)$$

where $\alpha = \frac{1}{2}j\Delta x$ and $\beta = \frac{1}{2}l\Delta y$.

After taking the determinant of equations (A.9) - (A.11) and simplifying, the quadratic

$$(\xi - 1)[(\xi - 1) + wB] + \xi A = 0 \qquad (A.12)$$

is obtained where

$$A = 4(\mu^2\sin^2\alpha\cos^2\beta + \nu^2\sin^2\beta\cos^2\alpha) \qquad (A.13)$$

$$B = 4(\mu^2 + \nu^2)\sin^2\alpha\sin^2\beta \qquad (A.14)$$

$$\mu^2 = gH\frac{\delta t^2}{\Delta x^2} \quad \text{and} \quad \nu^2 = gH\frac{\delta t^2}{\Delta y^2}$$

The solution of equation (A.12) is thus

$$\xi = 1 - \tfrac{1}{2}(A + wB) + [(A + wB)^2 - A]^{\frac{1}{2}} \qquad (A.15)$$

There are several possible solutions to this equation, but since A, B and w are all positive quantities the modulus of the amplification factor is given by

$$|\xi| = \tfrac{1}{2}(A + wB) - 1 + [(A + wB)^2 - A]^{\frac{1}{2}} \qquad (A.16)$$

For stability we require that $|\xi| \leq 1$, that is

$$\tfrac{1}{2}(A + 2wB)^{\frac{1}{2}} \leqslant 1 \qquad (A.17)$$

After substituting from equations (A.13) and (A.14), this implies that

$$\mu^2 \sin^2\alpha \cos^2\beta + \nu^2 \sin^2\beta \cos^2\alpha + 2w(\mu^2+\nu^2) \sin^2\alpha \sin^2\beta \leqslant 1 \qquad (A.18)$$

and so a necessary condition for stability is

$$w \leqslant \frac{1 - \mu^2 \sin^2\alpha \cos^2\beta + \nu^2 \sin^2\beta \cos^2\alpha}{2(\mu^2+\nu^2) \sin^2\alpha \sin^2\beta} \qquad (A.19)$$

An upper limit of $w = 0.25$ may be obtained from (A.19) by taking $\sin^2\alpha = \sin^2\beta = 1$, provided that the choice of gridlength and timestep is such that the C.F.L criteria of $\mu^2 < 1$ and $\nu^2 < 1$ are satisfied.

The condition for stability in the x-direction may be obtained from equation (A.16). When $\mu^2 > \nu^2$ and $0 \leqslant w \leqslant 0.25$, then $\cos^2\beta = 1$ gives

$$\mu^2 \sin^2\alpha \leqslant 1 \qquad (A.20)$$

for stability. This result is true for all values of ℓ, the wavenumber in the y-direction.

A.3 <u>The advection step</u>

A linear stability analysis for the modified Lax-Wendroff scheme has been given by Gadd (1978b) and (1980). When this scheme is applied to the two-dimensional linear advection equation

$$\frac{\partial\theta}{\partial t} + u\frac{\partial\theta}{\partial x} + v\frac{\partial\theta}{\partial y} = 0 \qquad (A.21)$$

the amplification factor for a typical Fourier mode is is given by

$$\xi = 1 - 2\delta^2 A^2 [1 + (1-\delta^2)C] - 2i\eta\delta A [1 + (1-\delta^2)C] \qquad (A.22)$$

where $A = \cos\phi \sin\alpha \cos\beta + \sin\phi \cos\alpha \sin\beta$;

$C = \sin^2\alpha + \sin^2\beta - \frac{4}{3}\sin^2\alpha \sin^2\beta$;

$\eta = \cos\alpha \cos\beta$;

$$\phi = \tan^{-1}(\nu/\mu) \; ;$$

$$\mu = u\Delta t/\Delta x \; ; \quad \nu = v\Delta t/\Delta y \; ; \quad \delta^2 = \mu^2 + \nu^2 \; ;$$

$$\alpha = \tfrac{1}{2} j \Delta x \; ; \quad \beta = \tfrac{1}{2} l \Delta y \; .$$

Equations governing the stability properties of the scheme in the x-direction may be obtained by setting $\cos\beta = 1$ in equation (A.23). This gives

$$\xi = 1 - 2\delta^2\cos^2\phi\sin^2\alpha\,[1+(1-\delta^2)\sin^2\alpha] - 2i\,\delta\cos\phi\sin\alpha\cos\alpha\,[1+(1-\delta^2)\sin^2\alpha]$$

so that, after some algebra,

$$|\xi| = [1 - 4\mu^2[\nu^2 + (1-\mu^2)(1-\delta^2)\sin^2\alpha\,](1+(1-\delta^2)\sin^2\alpha)\sin^4\alpha\,] \qquad \text{(A.23)}$$

This formula provides an upper bound for the amplification factor for all wavenumbers l in the y-direction.

An analysis of equation (A.23) shows that the scheme is stable in the x-direction provided that

$$\delta^2 \leq 1 + \frac{1}{\sin^2\alpha} \; , \qquad \text{(A.24)}$$

a higher level of stability than predicted by the C.F.L criterion.

APPENDIX B.

Radiation constants

This section tabulates the constants used by the climatological radiation scheme (see Section 8). These are specified at 10^{o} latitude intervals and in the case of atmospheric functions at 200 mb intervals for each solstice and equinox. Unless otherwise indicated the tables apply equally to both the Northern Hemisphere and the Southern Hemisphere.

Simple linear interpolation between latitude bands and between pressure levels is used in the model to derive the value of a function at any spatial position. Interpolation is also carried out in time. This ensures that the correct solar heating and long wave cooling rates are specified for the time of year of the forecast. The sinusoidal variation in the values of the mean solar heating and long wave cooling rates is modelled by using the solstice values for the 30 days before and after the solstice. At other times linear interpolation between adjacent solstice and equinox values is used.

Table B.1. Total column emissivities.

Latitude (^{o})	0	10	20	30	40	50	60	70	80	90
Winter solstice	.910	.918	.928	.937	.942	.946	.949	.950	.952	.952
Spring equinox	.911	.915	.923	.931	.937	.942	.946	.949	.951	.952
Summer solstice	.910	.910	.918	.927	.935	.940	.944	.947	.949	.950
Autumnal equinox	.911	.914	.920	.928	.933	.937	.941	.943	.947	.947

Table B.2. Surface solar flux in W m^{-2} day^{-1}.

Latitude (°)	0	10	20	30	40	50	60	70	80	90
Winter solstice	227.	222.	199.	148.	93.6	52.3	21.3	0.	0.	0.
Spring equinox	235.	264.	284.	263.	223.	193.	171.	180.	160.	140.
Summer solstice	227.	249.	273.	295.	277.	237.	218.	230.	230.	230.
Autumnal equinox	235.	224.	221.	194.	144.	94.5	56.	27.2	2.9	0.

Table B.3. Surface albedo.

Latitude (°)	0	10	20	30	40	50	60	70	80	90
Northern Hemisphere	.146	.188	.225	.212	.207	.170	.149	.180	.180	.180
Southern Hemiphere	.146	.173	.201	.224	.190	.190	.190	.190	.190	.190

Table B.4 Surface radiative exchange coefficients 10^{-9} W m^{-2} K^{-4}

Latitude (°)	0	10	20	30	40	50	60	70	80	90
Northern Hemisphere	11.43	11.19	10.61	9.793	8.996	8.126	7.437	6.772	6.350	5.810
Southern Hemisphere	11.43	11.95	11.78	11.44	10.75	10.30	9.844	9.160	7.910	6.700

Table B.5. Long wave cooling coefficients in 10^{-10} K^{-3} $days^{-1}$.

Latitude (°)	0	10	20	30	40	50	60	70	80	90
1000 - 800 mb										
Winter solstice	2.69	2.76	2.86	3.1	3.29	3.48	3.5	3.34	3.17	3.12
Spring equinox	2.71	2.76	2.9	3.07	3.29	3.53	3.65	3.6	3.17	3.17
Summer solstice	2.69	2.71	2.86	3.0	3.22	3.46	3.70	3.65	3.34	3.36
Autumnal equinox	2.71	2.71	2.76	2.93	3.10	3.34	3.38	3.36	3.31	3.24
800 - 600 mb										
Winter solstice	3.65	3.77	3.94	4.22	4.44	4.68	4.70	4.56	4.39	4.34
Spring equinox	3.67	3.74	3.96	4.15	4.44	4.68	4.82	4.80	4.37	4.37
Summer solstice	3.65	3.67	3.86	4.06	4.32	4.61	4.87	4.82	4.54	4.54
Autumnal equinox	3.67	3.72	3.79	4.01	4.20	4.46	4.54	4.54	4.49	4.44
600 - 400 mb										
Winter solstice	4.82	4.61	4.34	4.25	4.27	4.34	4.27	4.06	3.82	3.74
Spring equinox	4.82	4.73	4.54	4.44	4.44	4.51	4.51	4.32	3.84	3.82
Summer solstice	4.82	4.82	4.68	4.63	4.44	4.51	4.63	4.44	4.08	4.06
Autumnal equinox	4.82	4.73	4.54	4.42	4.42	4.49	4.42	4.30	4.15	4.03
400 - 200 mb										
Winter solstice	6.05	5.62	5.04	4.68	4.61	4.54	4.39	4.13	3.82	3.77
Spring equinox	6.02	5.81	5.38	5.06	4.87	4.82	4.68	4.44	3.91	3.86
Summer solstice	6.05	6.05	5.69	5.28	4.97	4.90	4.87	4.61	4.20	4.15
Autumnal equinox	6.02	5.83	5.47	5.14	5.02	4.92	4.78	4.38	4.30	4.20
200 - 0 mb										
Winter solstice	3.17	3.07	3.00	3.05	3.17	3.29	3.24	3.07	2.83	2.81
Spring equinox	3.17	3.14	3.12	3.14	3.24	3.38	3.43	3.31	2.86	2.86
Summer solstice	3.17	3.17	3.17	3.17	3.22	3.63	3.53	3.38	3.10	3.07
Autumnal equinox	3.17	3.12	3.07	3.07	3.14	3.29	3.26	3.19	3.07	3.00

Table B.6 Solar heating in K day .

Latitude ( )	0	10	20	30	40	50	60	70	80	90
1000 - 800 mb										
Winter solstice	.568	.585	.501	.376	.262	.240	.103	0	0	0
Spring equinox	.706	.769	.739	.628	.576	.510	.658	.597	.494	.391
Summer solstice	.568	.623	.664	.716	.693	.723	1.096	1.199	1.199	1.199
Autumnal equinox	.706	.660	.556	.468	.339	.266	.255	.132	.014	0
800 - 600 mb										
Winter solstice	.999	.945	.780	.653	.488	.273	.112	0	0	0
Spring equinox	1.023	1.036	1.094	1.035	1.070	.983	.708	.533	.439	.325
Summer solstice	.999	1.067	1.108	1.169	1.257	1.409	1.188	1.279	1.279	1.279
Autumnal equinox	1.023	.941	.879	.752	.658	.499	.305	.143	.016	0
600 - 400 mb										
Winter solstice	1.035	.809	.653	.513	.378	.219	.088	0	0	0
Spring equinox	1.059	1.010	.916	.893	.863	.843	.669	.480	.408	.336
Summer solstice	1.035	1.103	1.131	1.114	1.140	1.049	.979	.970	.970	.970
Autumnal equinox	1.059	.998	.854	.704	.564	.438	.270	.110	.015	0
400 - 200 mb										
Winter solstice	.883	.607	.477	.374	.265	.147	.077	0	0	0
Spring equinox	.783	.734	.665	.657	.631	.479	.468	.337	.314	.291
Summer solstice	.883	.936	.899	.897	.829	.819	.733	.688	.688	.688
Autumnal equinox	.783	.738	.635	.542	.411	.320	.172	.089	.011	0
200 - 0 mb										
Winter solstice	.550	.493	.439	.426	.396	.316	.204	0	0	0
Spring equinox	.626	.658	.686	.706	.755	.728	.799	.782	.875	.968
Summer solstice	.550	.589	.681	.659	.721	.795	.852	.961	.961	1.961
Autumnal equinox	.626	.587	.556	.520	.488	.431	.363	.223	.050	0

APPENDIX C.

Saturation specific humidity calculation.

The formula used for the calculation of the saturation specific humdity at pressure p and temperature T is

$$r_s(T, p) = \frac{0.622\, e_s(T)}{p}, \qquad (C.1)$$

where $e_s(T)$ is the saturation vapour pressure and is calculated in the model by linear interpolation from the values given in Table C.1. Note that if $T < -90^{\circ}C$ then $e_s(T) = 9.672\ 10^{-5}$ mb.

°C	SATURATION VAPOUR PRESSURE					
-90	$9.672\ 10^{-5}$	$1.160\ 10^{-4}$	$1.388\ 10^{-4}$	$1.658\ 10^{-4}$	$1.977\ 10^{-4}$	$2.353\ 10^{-4}$
-84	$2.796\ 10^{-4}$	$3.316\ 10^{-4}$	$3.925\ 10^{-4}$	$4.638\ 10^{-4}$	$5.472\ 10^{-4}$	$6.444\ 10^{-4}$
-78	$7.577\ 10^{-4}$	$8.894\ 10^{-4}$	$1.042\ 10^{-3}$	$1.220\ 10^{-3}$	$1.425\ 10^{-3}$	$1.662\ 10^{-3}$
-72	$1.936\ 10^{-3}$	$2.252\ 10^{-3}$	$2.615\ 10^{-3}$	$3.032\ 10^{-3}$	$3.511\ 10^{-3}$	$4.060\ 10^{-3}$
-66	$4.688\ 10^{-3}$	$5.406\ 10^{-3}$	$6.225\ 10^{-3}$	$7.159\ 10^{-3}$	$8.223\ 10^{-3}$	$9.432\ 10^{-3}$
-60	$1.080\ 10^{-2}$	$1.236\ 10^{-2}$	$1.413\ 10^{-2}$	$1.612\ 10^{-2}$	$1.838\ 10^{-2}$	$2.092\ 10^{-2}$
-54	$2.380\ 10^{-2}$	$2.703\ 10^{-2}$	$3.067\ 10^{-2}$	$3.476\ 10^{-2}$	$3.935\ 10^{-2}$	$4.449\ 10^{-2}$
-48	$5.026\ 10^{-2}$	$5.671\ 10^{-2}$	$6.393\ 10^{-2}$	$7.198\ 10^{-2}$	$8.097\ 10^{-2}$	$9.098\ 10^{-2}$
-42	$1.021\ 10^{-1}$	$1.145\ 10^{-1}$	$1.283\ 10^{-1}$	$1.436\ 10^{-1}$	$1.606\ 10^{-1}$	$1.794\ 10^{-1}$
-36	$2.002\ 10^{-1}$	$2.233\ 10^{-1}$	$2.488\ 10^{-1}$	$2.769\ 10^{-1}$	$3.079\ 10^{-1}$	$3.421\ 10^{-1}$
-30	$3.798\ 10^{-1}$	$4.213\ 10^{-1}$	$4.669\ 10^{-1}$	$5.170\ 10^{-1}$	$5.720\ 10^{-1}$	$6.323\ 10^{-1}$
-24	$6.985\ 10^{-1}$	$7.709\ 10^{-1}$	$8.502\ 10^{-1}$	$9.370\ 10^{-1}$	1.032	1.135
-18	1.248	1.371	1.506	1.652	1.811	1.984
-12	2.172	2.376	2.597	2.889	3.097	3.522
-6	3.8619	4.2148	4.5451	4.8981	5.2753	5.678
0	6.1078	6.5662	7.0547	7.5753	8.1294	8.7192
6	9.3465	10.013	10.722	11.474	12.272	13.119
12	14.017	14.969	15.977	17.044	18.173	19.367
18	20.630	21.964	23.373	24.861	26.430	28.086
24	29.831	31.671	33.608	35.649	37.796	40.055
30	42.430	44.927	47.551	50.307	53.200	56.236
36	59.422	62.762	66.264	69.934	73.777	77.803
42	82.015	86.423	91.034	95.855	100.89	106.16
48	111.66	117.40	123.40	129.65	136.17	142.98
54	150.07	157.46	165.16	173.18	181.53	190.22
60	199.26	208.67	218.45	228.61	239.18	250.16

Table C.1. Saturation vapour pressure (mb) at temperature T (°C). Values are for saturation over ice when $T \leq -8^{\circ}C$ and for saturation over water when $T \geq -5^{\circ}C$, with transitional values used for $-8^{\circ}C < T < -5^{\circ}C$.

APPENDIX D.

Surface characteristics.

This section describes the orography and climatic types used in the operational forecast models.

D.1. Model orography.

The global orography used in the coarse-mesh model has been derived by interpolation from a dataset of half-degree gridbox mean values provided by the United States Air Force. Some further smoothing has then been carried out over Antartica and Greenland. See Figure D.1.

The fine-mesh orography is derived by a simple bi-linear interpolation of the global orography.

D.2. Climatic types.

The six surface climatic types used in the models are: temperate land, sea, sea-ice, land-ice, arid-land and snow-covered land. These are modified each month to reflect the seasonally changing patterns. The values used operationally are given in Figures D.2 - D.13.

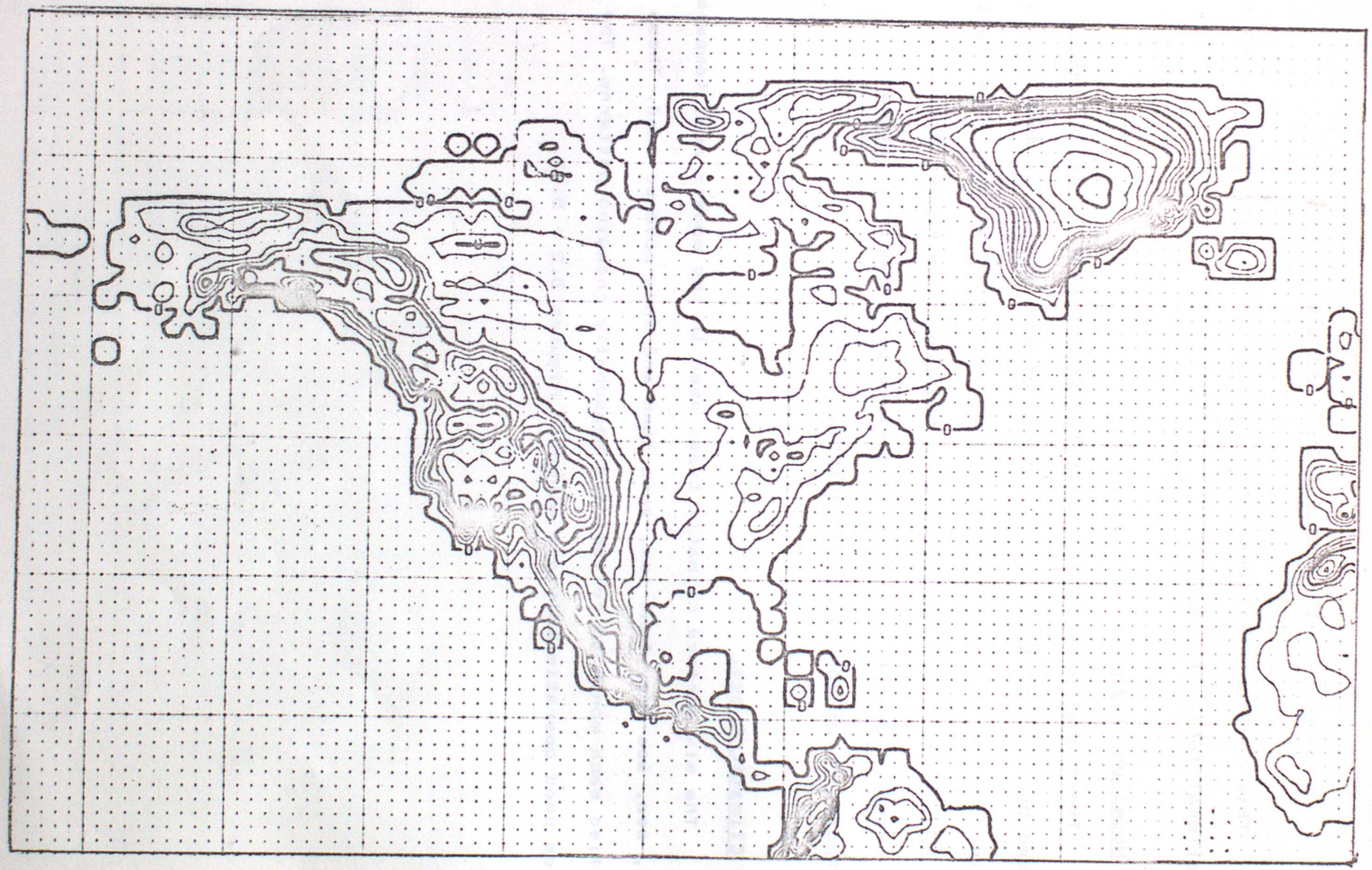

Figure D.1. Global model orography.

Contour interval = 250 m .

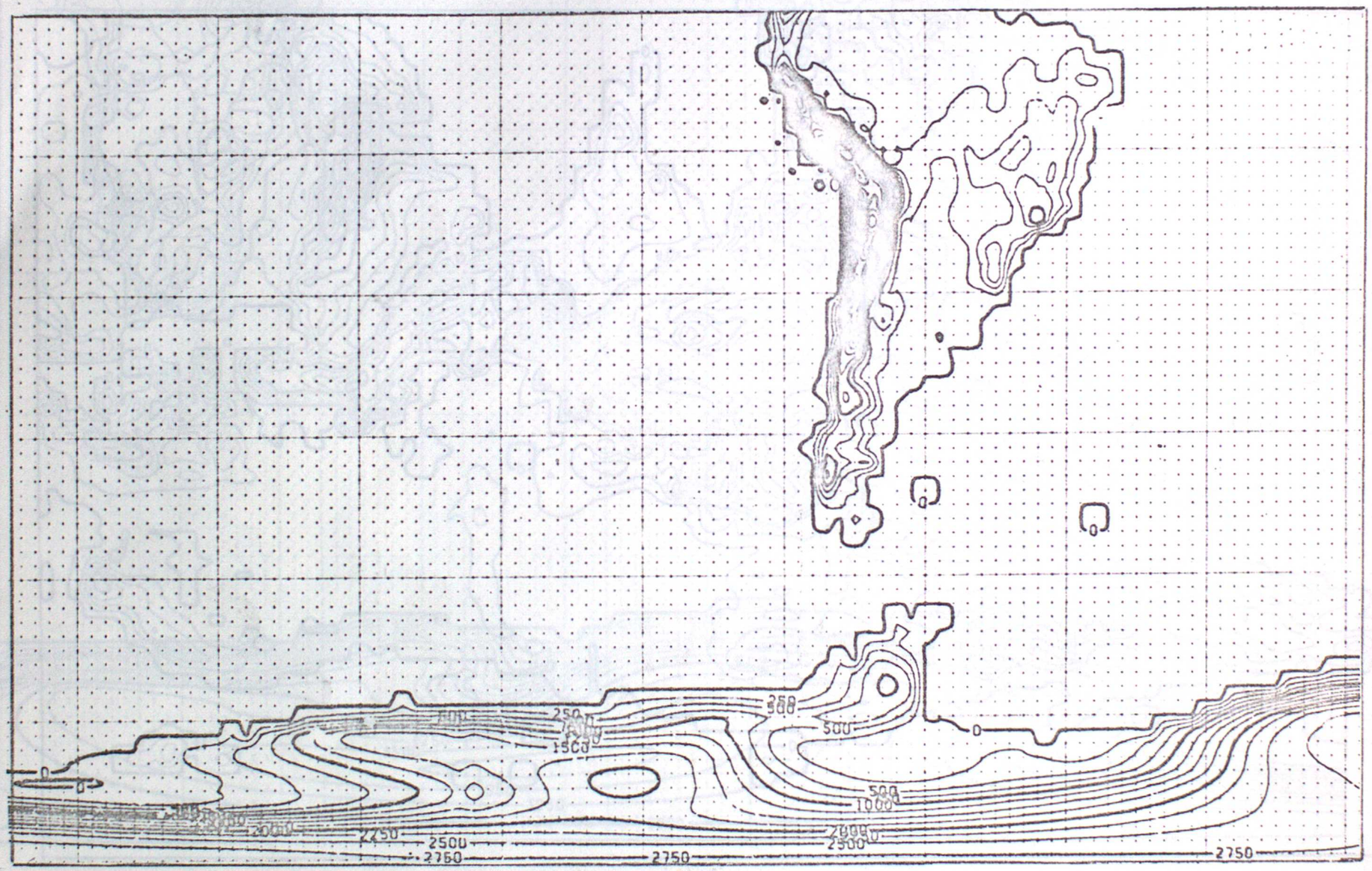

Figure D.1. Global model orography (continued).

Contour interval = 250 m.

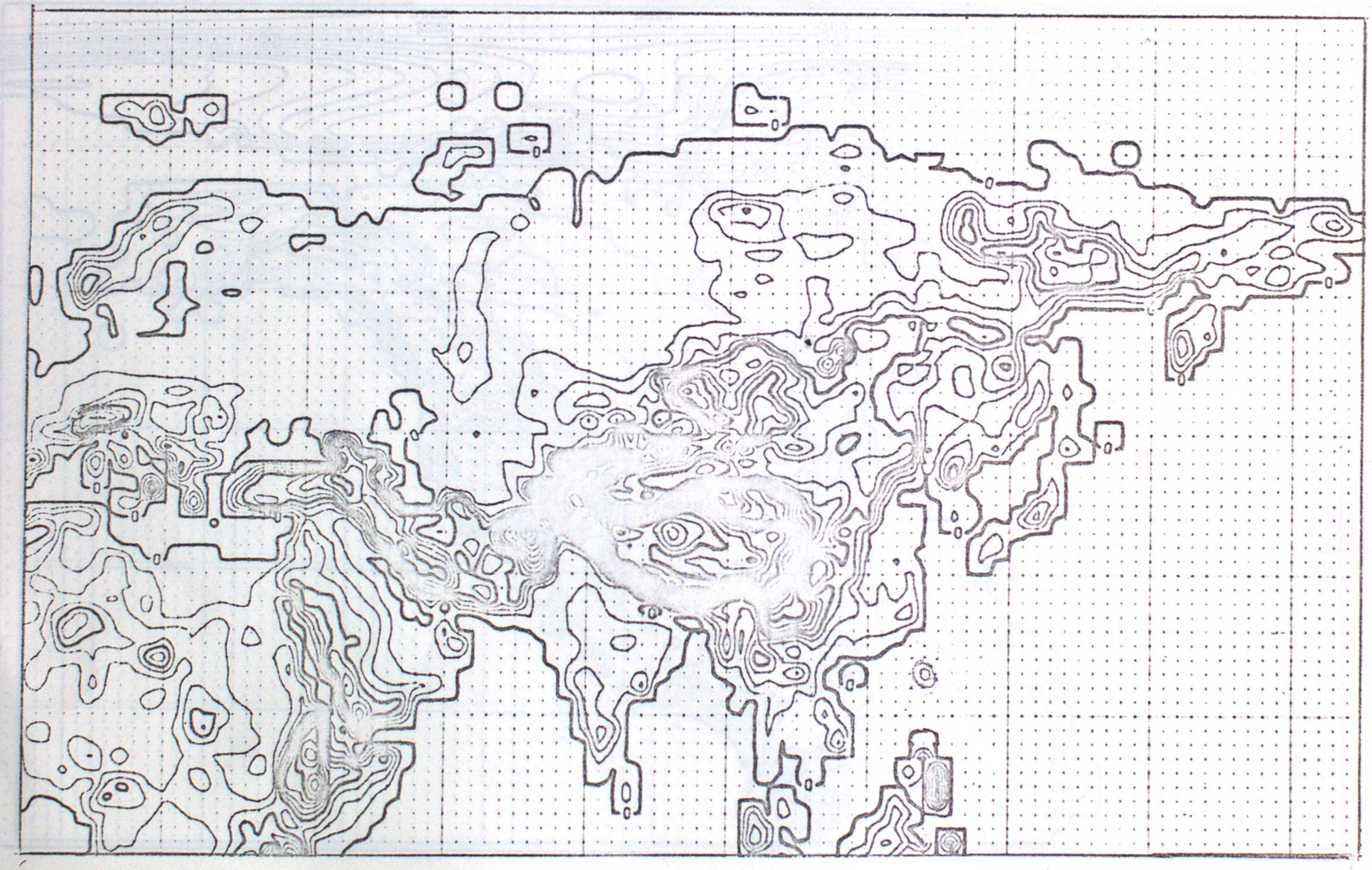

Figure D.1. Global model orography (continued). Contour interval = 250 m.

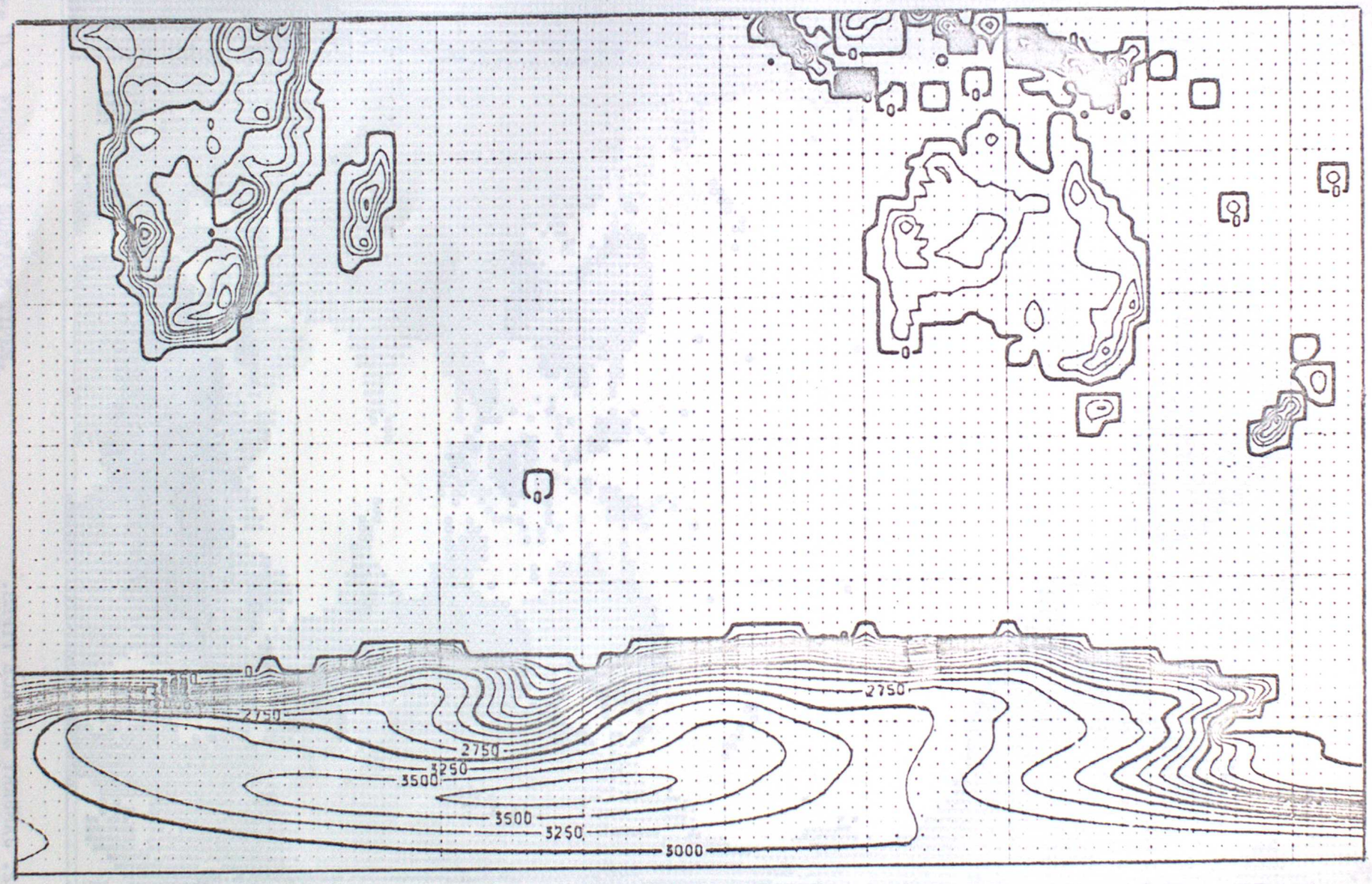

Figure D.1. Global model orography (continued).

Contour interval = 250 m .

Figure D.2. JANUARY SURFACE TYPES.

Temperate land = ⊙ ; Sea-ice = ∧ ; Land-ice = ⧋ ; Arid-land = ⊡ ; Snow covered land = ✳

Figure D.3. FEBRUARY SURFACE TYPES.

Temperate land = ⓪ ; Sea-ice = ∧ ; Land-ice = ⧋ ; Arid land = ⊡ ; Snow covered land = ✳

Figure D.4. MARCH SURFACE TYPES.

Temperate land = ⓪ ; Sea-ice = ∧ ; Land-ice = ⧋ ; Snow covered land = ✳ ; Arid land = ⊡

Figure D.5. APRIL SURFACE TYPES.

Temperate land = ⓪; Sea-ice = Λ; Land-ice = ⍋; Snow covered land = ✳; Arid land = ⍐

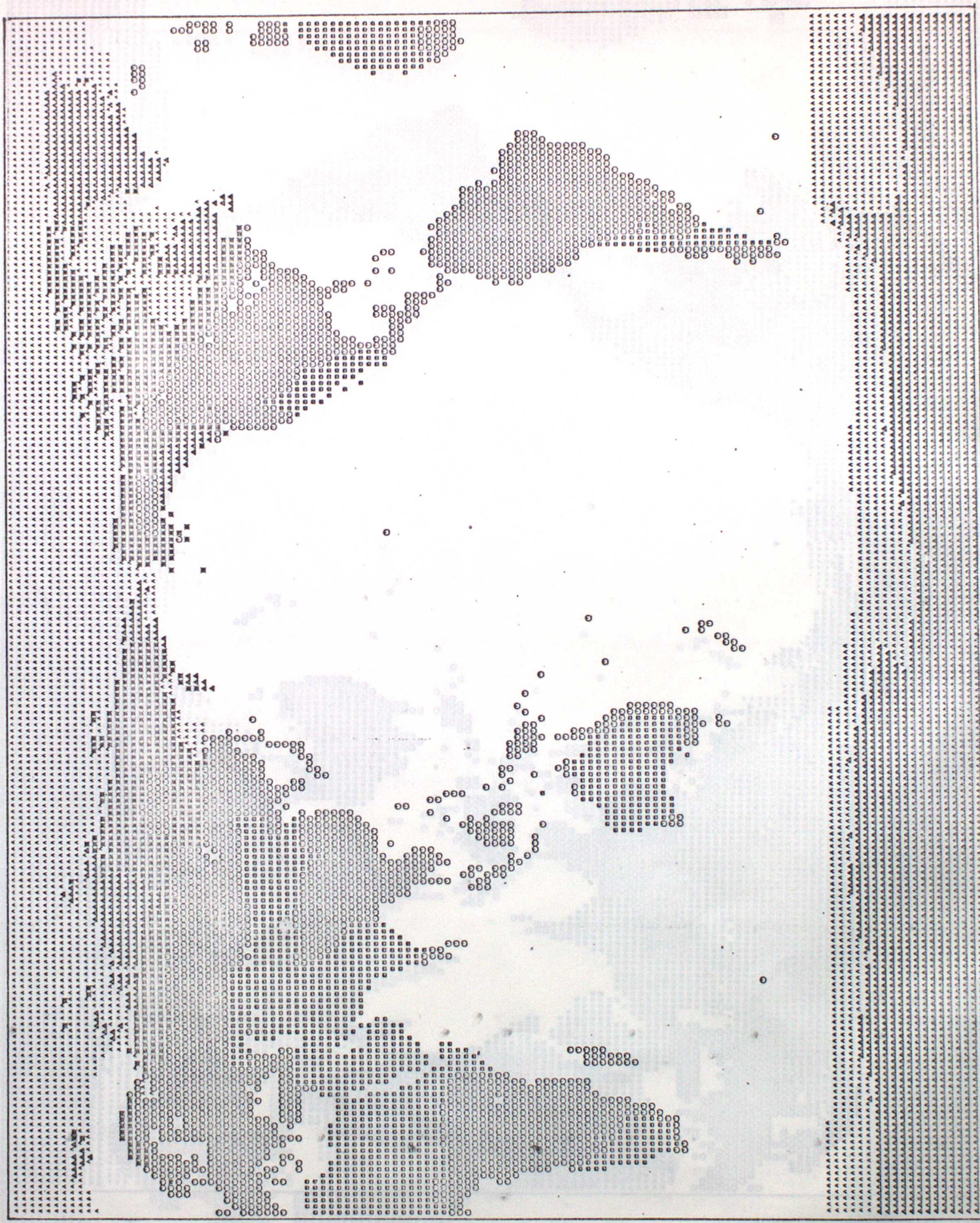

Figure D.6. MAY SURFACE TYPES.

Temperate land = Θ; Sea-ice = Λ; Land-ice = ⍋; Snow covered land = ✳; Arid land = ⍞

Figure D.7. JUNE SURFACE TYPES.

Temperate land = ⏀ ; Sea-ice = Λ ; Land-ice = Δ ; Snow covered land = ✳ ; Arid land = ⍓

Figure D.8. JULY SURFACE TYPES.

Temperate land = ⓣ; Sea-ice = ⋀; Land-ice = ⧋; Snow covered land = ✳; Arid land = ⊡

Figure D.9. AUGUST SURFACE TYPES.

Temperate land = ⓪; Sea-ice = Λ; Land--ice = ⚠; Snow covered land = ✳; Arid land = ⚅

Figure D.10. SEPTEMBER SURFACE TYPES.

Temperate land = ⓪; Sea-ice = Λ; Land-ice = ◮; Snow covered land = ✳; Arid land = ⊡

Figure D.11. OCTOBER SURFACE TYPES.

Temperate land = ⓪; Sea-ice = ∧; Land-ice = ⍋; Snow covered land = ✳; Arid land = ⍞

Figure D.12. NOVEMBER SURFACE TYPES.

Temperate land = ⊙; Sea-ice = ⩚; Land-ice = ⩓; Snow covered land = ✳; Arid land = ⊡

Figure D.13. DECEMBER SURFACE TYPES.

Temperate land = ⓪ ; Sea-ice = Λ ; Land-ice = ⍋ ; Snow covered land = ✳ ; Arid land = ⍓